Spatial and Spectral Photoluminescence Characterisation of Semiconductor Wafers

A thesis for the degree of

Master of Science

Submitted to

Dublin City University

by

Shane Francis White B.Sc.

Research Supervisor

Prof. Martin Henry

School of Physical Sciences

Dublin City University

March 1996

Declaration

I hereby certify that this material, which I now submit for assessment on the programme of study leading to the award of Master of Science is entirely my own work and has not been taken from the work of others save and to the extent that such work has been cited and acknowledged within the text of my work.

Signed: Shane White Date: 20/3/96

Shane White

Table of Contents

Acknowledgements

Initially I would like to thank my supervisor Prof. Martin Henry for all his support and help throughout this project. I would also like to thank the following people for making my time in D.C.U an interesting and informative one; Enda, Siobhan, Will, Andy, John, Kate, Dirk, Pat, Aisling, Fidelma, Charles, Marian, Al and Des.

To my friends outside D.C.U, in particular John Cahill, Derek, Dara and Mike, I thank you for the many distractions.

Finally I dedicate this thesis to my parents for they have shown me the true meaning of the word sacrifice.

Abstract

This work describes the development of a facility for the spatial and spectral analysis of semiconductor wafers at cryogenic temperatures using photoluminescence (PL).

Wafers of up to 50mm in diameter can be placed in the custom-designed cryostat and held at any temperature between 2 and 300K. A scanning optical table is used to scan the excitation beam across the wafer and collect the resulting PL signal. The spatial resolution of this arrangement was verified as 600μm. Spectral analysis of the wafer is achieved using a CCD detector mounted on a grating spectrograph. Two separate detector/spectrograph systems were used during this project, both of which are described and compared. The maximum spectral resolution achieved was 1nm at wavelengths in the range 800 to 1000nm. From the spectral information such images as the peak intensity, peak wavelength and the full width at half maximum can be obtained. Several examples of peak wavelength and peak intensity maps of epilayer and quantum well structures grown on GaAs wafers recorded at room, liquid nitrogen and liquid helium temperatures are presented.

Chapter 1

Introduction and Theory

1.0 Introduction

Optoelectronics plays an important role in the development of the information revolution, from the use of semiconductor lasers and detectors in optical fibre communication to their use in optical storage, *i.e.* the CD-ROM. Optical storage is only at the early stages of development with various new techniques being investigated, such as holographic storage. Thus with this increasing dependence on optoelectronic devices the need for yield improvement assumes greater importance. Consequently there is a need to assess, at the various stages in the fabrication of optoelectronic devices, the quality of the elemental semiconductor materials.

Semiconductors are affected by the introduction of small amounts of impurities or compositional changes. It is this sensitivity to changes in the material which makes semiconductors attractive to the optoelectronic and electronic industries. For example, by varying the composition of In in InGaAs the energy associated with the band gap of this material can be altered with the result that the peak absorption or emission wavelength of this material can be tailored to meet design demands. This quality that makes semiconductors interesting creates its own problems in that small inadvertent changes, *i.e.* minute contamination during growth, have large affects on the material and ultimately influence the performance of the finished product. Hence the reason why it is necessary to be able to characterise and monitor the materials at the various stages in the development of a device.

There are three main categories that semiconductor characterisation falls into

- Electrical characterisation,
- Optical characterisation and
- Physical/chemical characterisation.

Electrical characterisation gives electrically relevant information, such as resistivity and carrier concentrations, but it generally does not uniquely identify

impurities unlike the other two methods. A major disadvantage with this form of characterisation is that it generally requires electrical contacts to be attached to the sample which renders the sample useless for further processing and it also limits the possibility of spatially probing samples.

Physical/chemical characterisation gives visual and structural information, compositional and defect parameters, and impurity identification. The methods associated with this characterisation are generally not very sensitive and they require for the most part elaborate equipment. An example of some of these characterisation methods are scanning electron microscopy and secondary ion mass spectroscopy. A detailed discussion of these characterisation methods can be found in [1,2].

Optical characterisation is useful in determining such parameters as physical device dimensions, layer thickness, impurity and defect identification and concentrations. The maturity of the laser industry has led to optical diagnostic tools becoming more accessible to physicists and R&D engineers. Optical characterisation has the following advantages over the other two characterisation categories :

- it is a non contact technique,
- it is non destructive,
- generally there is no need for elaborate equipment,
- it requires little sample preparation and
- it does not require special environments, such as a ultrahigh vacuum.

As a result of the non contact nature of optical characterisation, and the ease at which an optical beam can be manipulated, spatial mapping, with submicron resolution, of semiconductor wafers is very much a reality.

The following are the most widely used optical techniques :

- reflectivity and transmission, including ellipsometry, modulation spectroscopy and scatterometry.
- Raman scattering.
- photoluminescence (PL).
- Infrared spectroscopy.

With these techniques it is possible to measure various parameters of a semiconductor material. In Table 1.1 a list of semiconductor properties that can be characterised by

the last three optical characterisation techniques is given. More information on any of the aforementioned techniques is available in the references [3,4].

Semiconductor property	Optical method		
	PL	Raman	IR
Band			
Gap	•		•
Effective mass			•
Band offset	•		
Free carrier			
Concentration		•	•
Mobility		•	•
Scattering time		•	•
Resistivity		•	•
Lattice			
Alloy composition	•	•	•
Orientation		•	
Crystallinity	•	•	
Stress	•	•	
Impurity and defect			
Presence and type	•	•	•
Concentration	•	•	•
Microstructure			
Layer thickness			•
Surface behavior	•	•	
Interface behavior	•	•	•
Layer-by-layer behavior			•
Other			
Homogeneity mapping	•	•	•

Table 1.1 Semiconductor properties that can be characterised by photoluminescence, Raman scattering and infrared spectroscopy.

It is the intention of this thesis to describe an experimental apparatus that uses PL to spatially and spectrally map semiconductor wafers of 50mm in diameter or less at room and cryogenic temperatures, to discuss the results obtained with this system and to examine possible future applications of this system. This chapter deals with the theory behind PL, it gives a general outline of what is required for a wafer mapping system, it references some of the existing systems and finally it discusses the layout of the system designed for this project.

1.1 Photoluminescence Characterisation

Photoluminescence is the term given to the luminescence produced when a material has been excited by photons, usually a laser. In photoluminescence, an optical transition occurs from an excited electronic state to a lower electronic state. The PL resulting from a transition is characteristic of either intrinsic transitions or transitions at defects or impurities in the material. Thus PL is spectroscopic in nature, *i.e.* the intensity is monitored versus wavelength. The wavelength range assessed by PL lies between the ultra violet, visible and near infrared regions, ~0.4-1μm. The spectra of semiconductors within this range are determined to a great extent by the details of the conduction and valence band states and by the occurrence of energy levels within the band gap [5].

The band gap of semiconductors can be either a direct gap as in the case of gallium arsenide (GaAs) or an indirect gap as in the case of silicon (Si). For the direct gap if the sample is excited by a photon with an energy greater than the band gap then an electron-hole pair is created with the electron being excited to the conduction band leaving a hole in the valence band. The electron and hole generally then thermalise down to the conduction and valence band edges respectively. If the electron later radiatively recombines with the hole a photon will be emitted (PL) with an energy given by equation 1.1,

$$\hbar\omega = E_g + E_e + E_h \qquad (1.1)$$

where $\hbar\omega$ is the photon energy, E_g is the energy associated with a band to band transition and E_e and E_h are the electron and hole energies, respectively, measured from the corresponding band edge. At room temperature, the PL emission lies at approximately the band gap energy but extending slightly to higher energies due to the thermal energies of the recombining electron and hole. For an indirect gap material the recombination involves the loss or gain of momentum by the electron due to an interaction with a phonon and the energy of the emitted photon is given by equation 1.2,

$$\hbar\omega = E_g + E_e + E_h \pm \hbar\Omega \qquad (1.2)$$

where $\hbar\Omega$ is the energy of the momentum-conserving phonon and the plus and minus signs correspond to phonon absorption and emission respectively.

At low temperature and with low excitation densities the electron-hole pairs form a bound pair, called a free exciton, due to their Coulomb interaction. In high purity material where the number of defects and impurities that can trap excitons is low the free excitons recombine giving rise to free exciton luminescence. The energy associated with free exciton luminescence from, for example, an indirect gap material is given by equation 1.3,

$$\hbar\omega = E_g - E_x \pm \hbar\Omega \qquad (1.3)$$

where E_x is the exciton binding energy.

If the concentration of exciton traps such as donor and acceptor impurities increases in the material then the probability that the free excitons which diffuse through the material will be captured by the exciton traps increases. Excitons trapped at shallow donors or acceptors are bound with a binding energy of a few meV, roughly 1/10 of the donor or acceptor ionisation energy [6]. These bound-excitons recombine leading to impurity specific bound-exciton luminescence. The energy of a photon associated with bound-exciton luminescence is given by equation 1.4,

$$\hbar\omega = E_g - E_x - E_B(\pm\hbar\Omega) \qquad (1.4)$$

where E_B is the binding energy of the exciton to the neutral donor or acceptor. The reason for the brackets surrounding the phonon energy is that the bound-exciton decay may or may not involve the emission of a momentum-conserving phonon.

There are other radiative recombination pathways available to the electron hole pairs and there are also non-radiative recombination pathways available. For example Table 1.2 shows the possible recombination pathways for silicon that is excited at low temperatures by a laser with a photon energy above the band gap, *e.g.* an argon ion laser. For a more detailed discussion on electron-hole pair recombination refer to [6].

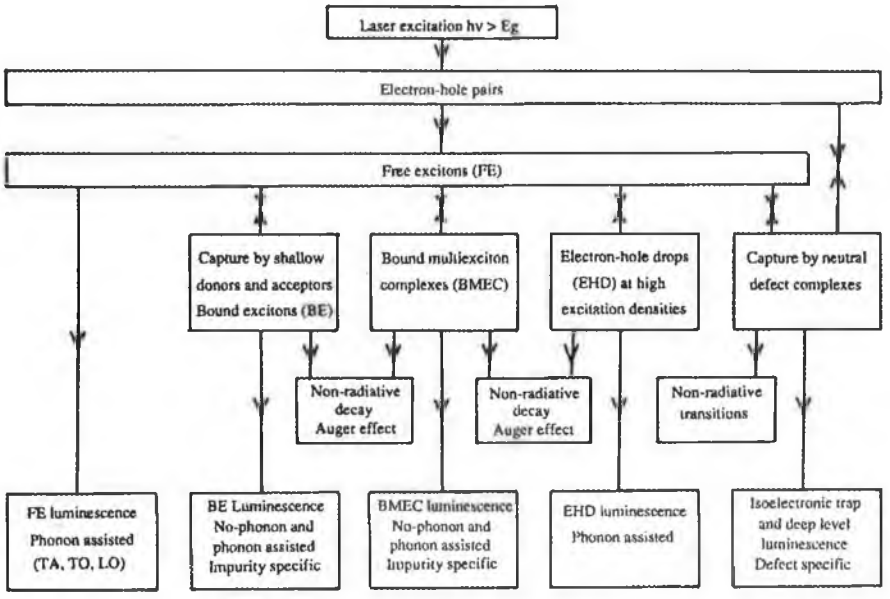

Table 1.2 Luminescence decay processes stimulated by above band gap photoexcitation.

Thus PL can be used to detect impurities and defects in materials and determine the purity of the material, *i.e.* the stronger the intensity of the free exciton luminescence the lower the concentration of shallow impurities. At this point it is worth noting that there is a certain depth to which the excitation beam can probe, called the penetration depth. Mathematically this is described as the distance into the sample at which the incident intensity falls to 1/e of its value at the surface of the semiconductor. It is dependent on the frequency of the probing beam and the semiconductor material being investigated. Typical values for penetration depths are between 0.1 and 1μm for silicon and 0.1μm for GaAs when using visible light as the excitation beam, as stated in [4]. Thus when using visible light PL spectroscopy is concerned with the investigation of near surface regions of semiconductor devices, which will in most cases cover the active region of an optoelectronic device. If, however, deeper probing is necessary infrared radiation could be used as the excitation source. Alternatively, the material could be probed by visible light at the different stages in the growth of the various epitaxial layers.

In the early stages of PL characterisation the work was mainly fundamental and mostly involved determining the various impurities and defects in a small section

of a semiconductor material. For optoelectronic devices, such as laser diodes, the tendency is to build them on whole wafers of III-V semiconductor materials, *i.e.* GaAs, or similar compound semiconductor materials. Consequently, it is now necessary to know how certain parameters vary spatially across a wafer. Examples of such parameters are changes in the alloy composition of ternary (AlGaAs) and quaternary (AlGaInP) materials or changes in the lasing wavelength of lasers made from this material. Thus there is an obvious need for whole wafer mapping at different stages in the development of these devices to be able to successfully counteract any deviation in the parameters and so lead to a greater yield of usable devices.

How can PL be used to yield such information about semiconductor material ? Figure 1.1 is a schematic illustration of a typical PL spectrum recorded at room temperature and on this spectrum are labelled the following parameters : the peak wavelength (λ_{peak}), the peak intensity (I_{peak}), the high side wavelength at which the intensity falls to 50% of the peak (λ_{+}) and the full width at half maximum (FWHM).

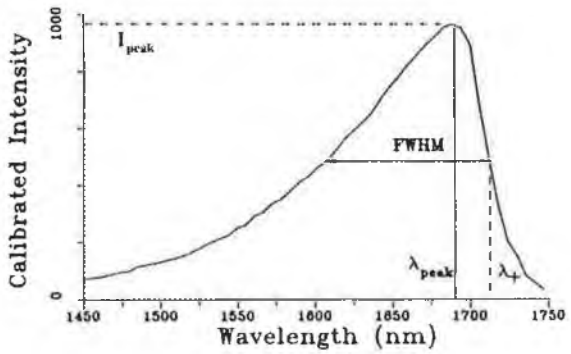

Figure 1.1 Typical room temperature PL spectrum obtained from an InGaAs epitaxial layer.

Changes in the peak wavelength may be due to a lot of different things such as variations in the composition of the alloy in ternary and quaternary epitaxial layers or due to variations in quantum-well widths. For example changes in the amount of aluminium (Al) in $Al_xGa_{1-x}As$ will alter the value of the peak wavelength by changing the energy associated with the band gap transition.

Equation 1.5 describes the quantized part of the electronic energy states of a quantum-well structure, quantized in the direction perpendicular to the plane of the epitaxial layers, *i.e.* the z direction.

$$E_n = \frac{\hbar^2}{2m}\left(\frac{n\pi}{L_z}\right)^2 \qquad n = 1,2,3.... \qquad (1.5)$$

As can be seen from the equation the energy is related to the well width (L_z). Thus deviations in the layer thickness causes variations in the energy levels which can manifest itself as a change in the value of the peak wavelength. Another advantage to knowing the peak wavelength is that it may be used to infer the lasing wavelength of the lasers built from these materials.

The peak intensity yields information on the purity and quality, *i.e.* the presence of competing radiative and/or non-radiative recombination centres, of semiconductor materials. Variations in the FWHM can be caused by a number of factors depending on the system under investigation including doping, layer disorder and layer grading effects [7]. The λ_+ also yields information about changes in the alloy composition of ternary and quaternary materials and is in many cases a better indicator, at room temperature, than the peak wavelength. The reason for this is that λ_+ is not sensitive to excitation power density unlike the peak wavelength, as discussed in [8].

1.2 PL Wafer Mapper

The apparatus which will be described should facilitate the two dimensional mapping of properties, such as alloy composition, across semiconductor wafers. The following are the most common basic requirements for such an apparatus :

1. An xy stage to facilitate the scanning of the whole wafer,
2. An excitation source and
3. A monochromator and detector.

In the case of the xy stage there are two ways in which this can be configured into the system. Either the wafer can be mounted on the stage and the optics held stationary or the wafer can be held stationary and the optics rastered across the wafer. Each configuration has its benefits and drawbacks. For example, in the first configuration the wafer is placed on the xy stage and this makes the mapping of

wafers at cryogenic temperatures a difficult procedure. The reason for this is that a large volume of space would have to be placed at low temperature in order to envelope the wafer and the xy stage whereas in the second configuration the wafer is the only item that has to be placed at low temperatures. On the other hand, keeping the optics stationary means that the excitation beam will remain focused on the sample at all points on the wafer, which can be difficult to maintain in the case of configuration two. Both methods have been successfully demonstrated [9,10].

The monochromator/detector combination is a very basic one and usually the detector is either a photodiode (*e.g.* a germanium detector) or a photomultiplier tube. This enables a spectrum to be recorded at various positions on the wafer. But recording the spectrum this way is time consuming, as it involves the rotation of a grating for the whole spectrum to be recorded by the single element detector. This has lead to the use of spectrographs in conjunction with photodiode arrays (PDA) or charged coupled device (CCDs). The advantage of this is that the PL signal is spectrally resolved instantly without having to move a grating and because the PDA and the CCD have detector arrays this spectrally resolved signal can be recorded immediately. Moretti *et al* successfully used a spectrograph/PDA detector configuration in their wafer mapping system, as described in [9]. Another benefit to using a CCD or PDA is that instead of recording the spectrum at various points on the wafer it is possible, using software, to extract and store in memory the relevant information (*e.g.* peak wavelength, peak intensity) from a spectrum in real time and then discard the spectrum.

The system that was developed during this project is based on different aspects of some of the previously mentioned systems. A spectrograph/CCD combination was used so as to facilitate real time measurement of spectra at the various points on the wafer. The wafer was held stationary and the excitation beam was guided across the wafer by use of mirrors and a motorised xy stage; see Figure 2.1 for a schematic diagram of the PL wafer mapping unit. Another slight variation on the basic wafer mapper design was that the wafer was placed in a bath cryostat. This means that the wafer could be cooled to any temperature between 2 and 300K. The advantage of this is that at lower temperatures thermal broadening of excited carrier energies is reduced, which is roughly k_BT for a temperature of T, where k_B is

Boltzmann's constant. This gives a significant broadening at room temperature of 25meV which is reduced to ~6meV at liquid nitrogen temperatures, and to < 1meV at liquid helium temperatures, as discussed in [4]. Therefore cooling the sample produces sharper more readily defined peaks and it also tends to give rise to a higher efficiency for the PL process resulting in a greater signal to noise ratio by reducing the role of non-radiative paths for recombination. Cooling prevents impurity centres from undergoing thermal ionisation. Also, cooling the sample may lead to the appearance of lines due to transitions via excitonic states and through intermediate states such as donors and acceptors as discussed in the previous section. Thus it is possible to monitor the distribution of various impurities and contaminants across the wafer [10].

There are other systems available that have the ability to attain low temperatures, one of which uses a closed cycle cryocooler rather than cryogenic liquids [11]. This has the advantage over a bath cryostat that wafer samples can be changed and brought to 15K in a short time interval, approximately 15 minutes, and that it doesn't use cryogens which are expensive. But it has the disadvantage that it can not go to temperatures lower than 15K whereas the bath cryostat used in this project can achieve temperatures as low as 2K.

1.3 Conclusions

Although electrical characterisation is still the mainstay in the semiconductor manufacturing industry for material specification there is a definite motivation for the use of optical characterisation due to its non destructive nature. Foremost among the optical techniques for semiconductor materials analysis is PL. The value of a facility which uses PL for monitoring the uniformity of various parameters across whole wafers is clear from the fact that there are at least two commercially available systems, *i.e.* the Waterloo Scientific SPM-200 [7] and the SCANTEK Scat Imageur [12], along with many other more research orientated systems. This project developed a system that is not a commercial product but it can supply a service of commercial value. This facility has the better points of all the previously mentioned systems, *i.e.* a whole spectrum can be recorded in real time at each point on the wafer and also maps can be recorded at temperatures between 2 and 300K.

In the next chapter each component of the wafer mapping facility and the software that co-ordinates the system is described.

References

1. G.E. McGuire, *Characterization of Semiconductor Materials Principles and Methods*, **Vol. 1**, Noyes Publications, New Jersey, 1989.
2. W.R. Runyan, *Semiconductor Measurements and Instrumentation* (Texas Instruments Series), McGraw-Hill, 1975.
3. P.M. Fauchet "Applied Optical Diagnostics of Semiconductors" *Proceedings of the IEEE*, **Vol. 80**, No. 3, pp. 420-435, March 1992.
4. S. Perkowitz *Optical Characterization of Semiconductors: Infrared, Raman and photoluminescence Spectroscopy*, Academic Press Limited, London, UK, 1993.
5. S. White, M.O. Henry, E. McGlynn, J.D. Lambkin and L. Considine "Imaging Semiconductor Wafers Using Photoluminescence" *Optical Engineering*, **Vol. 33**, No. 33, pp. 3974-3977, December 1994.
6. R.A. Stradling and P.C. Klipstein *Growth and Characterisation of Semiconductors*, pp. 135-163, Adam Hilger, Bristol, UK, 1990.
7. C.J.L. Moore and C.J. Miner "A Spatially Resolved Spectrally Resolved Photoluminescence Mapping System" *Journal of Crystal Growth*, **Vol. 103**, pp. 21-27, 1990.
8. I.C. Bassignana, C.J. Miner and N. Puetz "Photoluminescence and Double-Crystal X-Ray Study of InGaAs/InP: Effect of Mismatch Strain on Band Gap" *Journal of Applied Physics*, **Vol. 65**, Issue 11, pp. 4299-4305, June 1989.
9. A.L. Moretti, F.A. Chambers, G.P. Devane and F.A. Kish "Characterization of GaAs/$Al_xGa_{1-x}As$ Structures Using Scanning Photoluminescence" *IEEE Journal of Quantum Electronics*, **Vol. 25**, No. 5, pp. 1018-1024, May 1989.
10. M. Bugajski and J Ornoch "Photoluminescence Mapping: New Technique To Characterize Materials and Structures for Fabrication of Photonic Devices" *American Institute of Physics Conference Proceedings*, Part 227, pp. 38-41, 1991.
11. T.W. Steiner, M.L.W. Thewalt, M. Maciaszek and R.P. Bult "A Low-Temperature, Whole-Wafer-Imaging System for Defect and Impurity Mapping" *Canadian Journal of Physics*, **Vol. 69**, pp. 333-338, 1991.

12. M. Wolny, T. Duluc and C. Linne "Nondestructive Characterization of III-IV Materials for Infrared Detection by Scanned Photoluminescence" SPIE, **Vol. 2228**, pp. 332-341, 1994.

Chapter 2

Experimental Apparatus

2.0 Introduction

It is the intention of this chapter to describe each component of the experimental apparatus, as illustrated in Figure 2.1 and to give an account of the computer interfacing involved in co-ordinating the system. There were two separate spectrograph/detector systems used, both of which are discussed.

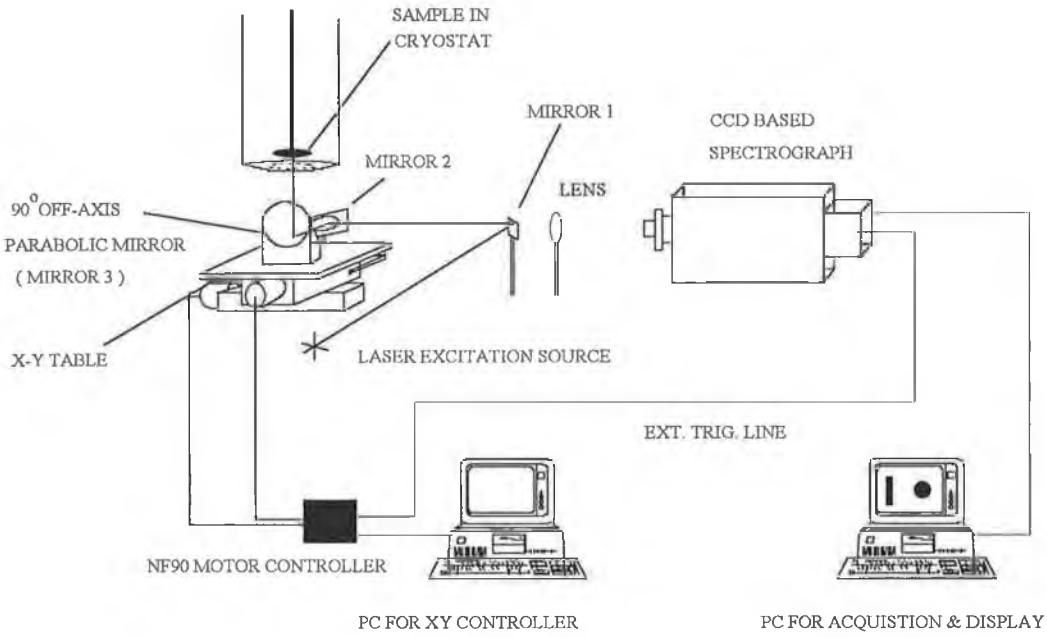

Figure 2.1 A schematic diagram of the wafer mapper set up.

2.1 Excitation Source.

The choice of excitation source is governed by certain requirements. It has to emit radiation of suitable wavelength so as to cause the semiconductor materials of interest to this project, *i.e.* GaAs and InP, to photoluminesce. It has to be directional so that it can be guided along the optical path of the set up. The spot size of the excitation beam dictates the dimensions of mirror 1 which by nature of its position in

the optical path, blocks part of the luminescence signal. Therefore an excitation source with a small spot size is advantageous.

An argon ion laser was selected as the source as it satisfied all the above requirements. This laser has more than one emission wavelength and this can cause problems if the PL signal appears at or near any of the emission wavelengths. To prevent this it is best to select one of the laser emission lines using a narrow bandpass interference filter. The laser line selected was the 514nm line. This emission line is then blocked from entering the spectrograph by placing a longpass filter in front of the spectrograph's entrance slit.

2.2 XY Translation Table.

The xy translation table is used in conjunction with the mirror assembly (see Section 2.3) to move the laser beam over the surface of the semiconductor sample. It comes with its own programmable stepper motor controller, called the NF90. This controller is programmed by computer via a RS-232-C connection. The computer commands used to control the motors are specific to the NF90 and permit the user to define the type of pattern in which the motors will be moved. The controller program used is discussed in Section 2.6.

The motors have a minimum step size of 5μm and a top speed of 2800-3000 steps per second or a 15mm per second translation rate. The maximum distance of travel for either axis of the translation table is ~152mm.

The translation table came with a remote manual push button control that allows the motors to be jogged or slewed to any xy position. This was particularly useful when spectra had to be obtained from different points on the wafer or when optically optimising the set up.

The translation table has two limit switches on each axis. One of the switches on each axis was positioned so as to define the x and y starting positions of all future wafer scans. This ensured that the whole wafer would be scanned each time.

2.3 Mirror Assembly

There are three mirrors in the system as shown in Figure 2.1. Mirror 1 is a plane mirror and its only purpose is to direct the laser beam onto mirror 2. Its area is

just greater than the laser spot size and it is mounted on a bar of 3mm in diameter, which is held in a rotating table. This arrangement allows the mirror face to be positioned so that the laser beam strikes the centre of mirror 2.

Mirror 2 directs the laser beam at mirror 3 and reflects the PL beam coming from mirror 3 to the spectrograph. Mirror 2 is a plane mirror which has an elliptical shape. The long axis is 113mm and the other axis is 80mm. This shape was decided upon because this mirror is placed at an angle of 45^0 to mirror 3 and at this orientation it acts like a circular shaped plane mirror of diameter 80mm. Thus it will reflect all of the 75mm diameter collimated PL beam coming from mirror 3.

Mirror 3 is an off axis paraboloidal reflector and by nature of its design reflects any parallel light beam striking it through 90^0 and brings this beam to a focus at the focal plane and vice versa; a more detailed discussion on the features of this mirror is given in [1]. Thus the laser beam coming from mirror 2 will be reflected upwards through 90^0 and focused at the wafer surface, which is at the focal plane. The PL emitting from the wafer will be collected by mirror 3, reflected back through 90^0 and collimated. This type of mirror was necessary because the laser beam had to remain in focus at the wafer surface, irrespective of the distance between mirror 2 and mirror 3. The reason for the movement between these two mirrors is to allow the laser beam to be scanned along the wafer in the direction perpendicular to the axis that contains mirror 1 and 2 and the spectrograph's entrance slit, see Figure 2.1. By moving mirror 2 along this axis the laser beam can be scanned across the wafer in the remaining direction. This combination of mirror motion causes the wafer to be raster scanned. As stated in Section 2.2 this motion is brought about by the xy translation table.

In summary, the laser beam is reflected in succession by mirrors 1,2 and 3 before being brought to a focus at the wafer surface and the PL emitted from the wafer is collected by mirror 3 and directed towards mirror 2, which in turn steers the collimated PL beam into the path of the spectrograph's entrance slit, as shown in Figure 2.2.

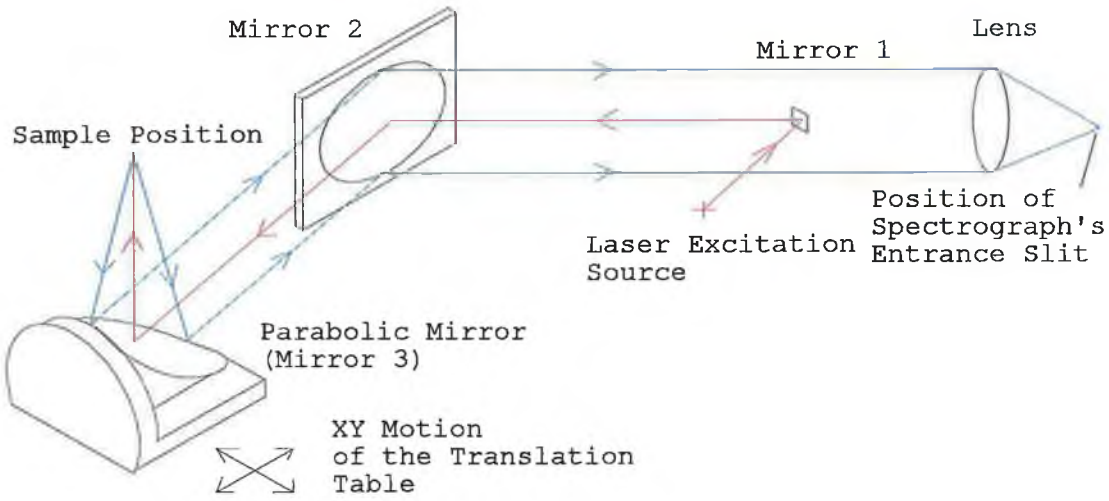

Figure 2.2 An isometric drawing of the mirror arrangement indicating also the direction of the PL signal (blue line) and laser beam (red line).

2.4 Cryostat

The cryostat, supplied by Janis Research Company, is a custom-designed detachable tail research dewar; see Figure 2.3 for a schematic diagram. It can hold 50mm diameter wafers.

The cryostat's sample mount was fitted with an 27Ω Rhodium-Iron (RhFe) resistance sensor which in turn was connected to a temperature controller (model ITC4), both supplied by Oxford Instruments. The ITC4 was also connected to the 25Ω heater on the sample mount. This temperature controller was specifically intended for use in cryogenic applications and by controlling the output of the heater the desired experimental temperature can be maintained. The ITC4 allowed the proportional, integral and differential control terms to be adjusted to maintain the temperature stability to within 0.1K. The RhFe sensor is usable in the temperature range 0.5K-300K.

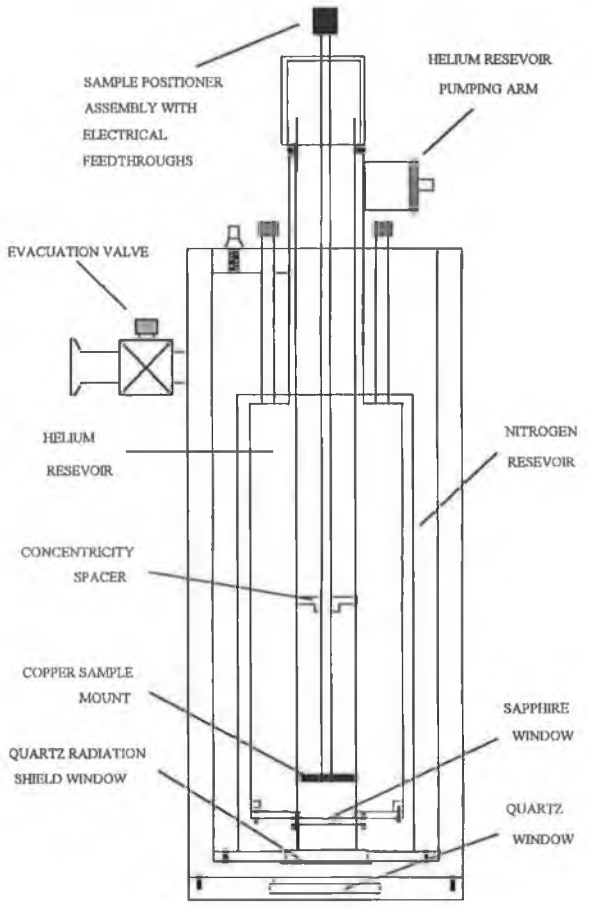

Figure 2.3 A schematic diagram of the Janis Cryostat.

This project only required that the samples be held at liquid nitrogen (77K) and liquid helium (4.2K) temperatures. The procedure for operating the cryostat to achieve these temperatures is described in detail in the cryostat manual [2].

It is worth noting, as mentioned in Chapter 1, that the sample can be brought to temperatures below 4.2K (~2K) by transferring liquid helium into the sample space and pumping on the sample space. Also temperatures between 4.2K and room temperature can be achieved. This is made possible by creating an adjustable "thermal link" between the sample and the liquid cryogen. The sample is placed in either an exchange gas or in vacuum. The latter allows any chosen temperature to be obtained without suffering heavy cryogen losses because of a poor "thermal link" between the sample and the liquid helium container. Using the ITC4 to control the power output of the heater on the sample mount any temperature within the previously specified range can be obtained. Liquid helium can be used to obtain temperatures between

4.2K and room temperature. Liquid nitrogen can be used to achieve temperatures between 77K and room temperature.

2.5 Spectrograph and Detector

In all, there were two spectrograph/detector combinations used for the duration of this project. The first combination was the InstaspecIV charged coupled device(CCD)/Multispec spectrograph, supplied by Andor Technology, and the second consisted of an OMA4 CCD detector combined with a 100S spectrograph, supplied by EG&G PARC and American Holographic, respectively.

The advantage of a CCD detector and spectrograph combination is that it allows a spectrum to be captured and analysed in a fraction of a second, as discussed in Section 1.2.

2.5.1 Charge Coupled Device

A CCD is a 2 dimensional array of photosensors. The array size of both CCDs used in this project was 1024 by 256 elements. The following paragraph gives a brief description of how a CCD works.

When the shutter is opened the photosensor array is exposed to a spectral source and photons strike the image face where they generate charge in the photosites (photosensors). Charge is collected over a period of time, called the exposure time, and then the shutter closes. The accumulated charge per photosite is then shifted one column at a time toward a serial transfer register, also called the shift register. This is accomplished by changing the potentials of the four electrodes buried under each potential well, a technique called four phase shifting. These electrodes define the photosite's area within the readout column. When a whole row has been placed in the shift register, the individual charges are shifted one by one to the video output of the CCD chip. The resultant analog signal is amplified, digitised, and can then be stored, displayed, or manipulated. Digitisation of the analog signal is achieved by an analog to digital converter (ADC). This ADC divides the range of analog signals from zero to saturation into a discrete number of levels; the number of levels is specified by the number of bits or binary digits, *e.g.* a 16 bit ADC corresponds to 65,536 levels.

The main source of noise in a CCD is in performing a readout. Thus instead of reading out each row individually, as in the case just described, it would be more beneficial if the rows could be grouped together and then read out, thereby reducing the number of readouts per frame. This is achieved using a technique called binning, in which the charges from several consecutive detector elements are summed in a single element (bin) on the chip before being read out. By binning the charge and then performing the readout, the noise of only one readout is associated with the signal, resulting in an increase in the sensitivity of the CCD at the expense of its resolution. By binning all the rows into one it is possible to emulate a photodiode array which has a sensitivity comparable to a photomultiplier tube, but a CCD will not be damaged by over exposure to bright light unlike a photomultiplier.

2.5.2 InstaspecIV and Multispec

The 77400 Multispec is a light weight, miniature sized spectrograph that has a focal length of 120mm and an f/number of 3.7. It suffers from minimal coma and has a flat focal field for diode arrays of up to 1 inch (25mm) in length; outside this region the flat focal field optics no longer holds true. This pseudo flat focal field is due to the spherical optics used and the crossed Czerney Turner configuration in which they are arranged, as can be seen in Figure 2.4.

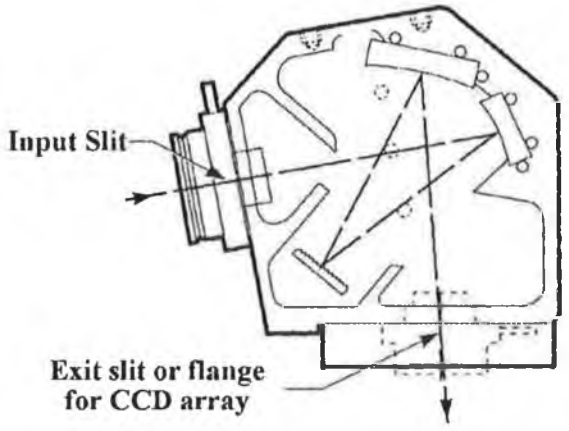

Figure 2.4 A diagram of the Multispec spectrograph.

This spectrograph does not support two dimensional imaging, a feature available to all CCDs. This was not a problem as two dimensional imaging was not

required for this system. In fact, the CCD was configured to emulate a photodiode array by use of binning as explained in the previous section.

A precision micrometer was used as the wavelength drive. This ensures a high degree of wavelength repeatability. The calibration for this micrometer was 1nm per graduation for a 1200 lines/mm grating. If a different grating is used the micrometer reading has to be multiplied by a conversion factor determined by the grating line density. To work out the wavelength range being viewed by the CCD all that is required is the present micrometer value; the software then calculates the wavelength range in view and displays it on the screen.

There is a large selection of interchangeable gratings available to cover the different spectral ranges. The grating used in this system was a ruled grating with 600 lines/mm and with a blaze wavelength of 750nm. It has a linear dispersion of 12nm/mm. The gratings are easily interchanged without the need to realign the instrument.

Instead of having a slit at the entrance to the spectrograph and focusing the luminescence on the slit, the luminescence was focused on an optical fibre bundle attached to the spectrograph. This was a rectangular to circular fibre bundle with a stainless steel sheathing. By attaching the fibre to the spectrograph the opening of the rectangular end of this fibre becomes the entrance slit of the spectrograph. Therefore the slit size in this case is 100μm by 2.5mm. The circular end has a SMA termination and the rectangular end has a 11mm quick connect ferrule. The fibre was made of glass, which has $90^0/_0$ transmission efficiency in the visible region.

The InstaspecIV CCD was designed specifically for spectroscopy in that the readout register is along the long axis. Therefore the best match of the spectrum image to the sensor area can be obtained by aligning the long axis along the dispersive plane of the spectrograph, *i.e.* the wavelength axis. The sensor has an area of 27.6mm by 6.9mm, 1024 by 256 elements, with no blind regions between the elements. The photosensitive material used was silicon. The spectral response of the CCD was 180nm to 1100nm. The ultra violet enhancement of the CCD was due to special coatings on the CCD. The CCD has an ultra low dark current, as a result of a technology called MPP, and when the CCD is thermoelectrically cooled it achieves a performance that standard devices, *e.g.* a germanium detector, can only obtain when

cooled by liquid nitrogen. MPP is a mode of operation of the CCD, also called the inverted mode, which suppresses the dark current by factors of 10 to 100 depending on the supplier. When operating a photodiode array it is necessary to bias the diode which causes a dark charge to build up in the substrate but with a CCD the individual photosensitive elements have to be biased only when a readout is to be performed. In the MPP mode the bias on the photosensitive element is inverted during non readout times causing the dark charge to be suppressed [4,5].

The CCD is cooled thermoelectrically by a single stage Peltier cooler. The heat generated by this Peltier device is dissipated with the aid of either air or water. If air is used it is possible to cool the CCD to roughly -5^0C, but if water is used temperatures as low as -25^0C can be achieved. Cooling the CCD will enhance its performance by reducing the dark current; the dark current is reduced by a factor of 2 for a 6^0C drop in temperature.

The typical noise per pixel is less than one count (one count is equal to 13 electrons) at 0^0C. This defines the minimum signal that can be measured. The maximum signal that can be detected is defined by the well depth or capacity of the pixel and for this CCD it is in excess of 800,000 electrons, *i.e.* of the order of 61,000 counts. Consequently, a 16 bit ADC (65,536 levels) is used to achieve optimum compatibility between the detector and the ADC, resulting in a maximum dynamic range of 65,536 : 1 for the system. For a comprehensive list of the specifications of the InstaspecIV see [5].

The CCD is computer controlled via a computer interface card and software, both of which are supplied by the manufacturers. The software facilitates spectra acquisition and extensive signal processing for one and two dimensional spectroscopy. It is also used to set the CCD's parameters, such as the exposure time, the CCD temperature and the number of rows to be binned. See Section 2.6 for a more detailed discussion of the computer interfacing technique used to co-ordinate the wafer mapping system.

The InstaspecIV comes with a multiple I/O accessory , model 77159, that enables the system to be connected to external instruments, such as a pulse source that could be used to trigger the CCD to acquire a spectrum. This I/O accessory is used as opposed to simply connecting directly to the CCD because it is an opto-

isolator. The opto-isolator filters any noise originating from the external apparatus and prevents a ground loop occurring between the CCD and external apparatus. Ground loops can be a big problem as they can give rise to interference, such as large voltages , appearing in digital signals.

This CCD/spectrograph system has the advantage that because it is a whole system, *i.e.* the CCD and spectrograph come as one attached unit, any necessary alignment between the CCD and spectrograph is performed by the manufacturer. Also the spatial distribution of light exiting from the spectrograph is suitably matched to the dimensions of the image zone of the CCD.

2.5.3 OMA4 and 100S Spectrograph

The American Holographic 100S spectrograph, as shown in Figure 2.5, has a flat focal plane and therefore is ideal for use with linear diode arrays or CCDs. It has a focal length of 0.1 meter and an aperture ratio of f/2.5. The spectrograph came with two gratings, two slits and a detector mount. The detector mount, model number DM-003, was the one which best suited the OMA4 detector. The two slit widths were 0.1mm and 0.05mm, model numbers SL-0100 and SL-0050 respectively. The gratings are aberration corrected holographic diffraction gratings. The first grating, model number 446.05/L, has a central wavelength of 485nm and an average dispersion of 8nm/mm. The second grating, model number 446.34/L, has a central wavelength of 750nm and an average dispersion of 20nm/mm.

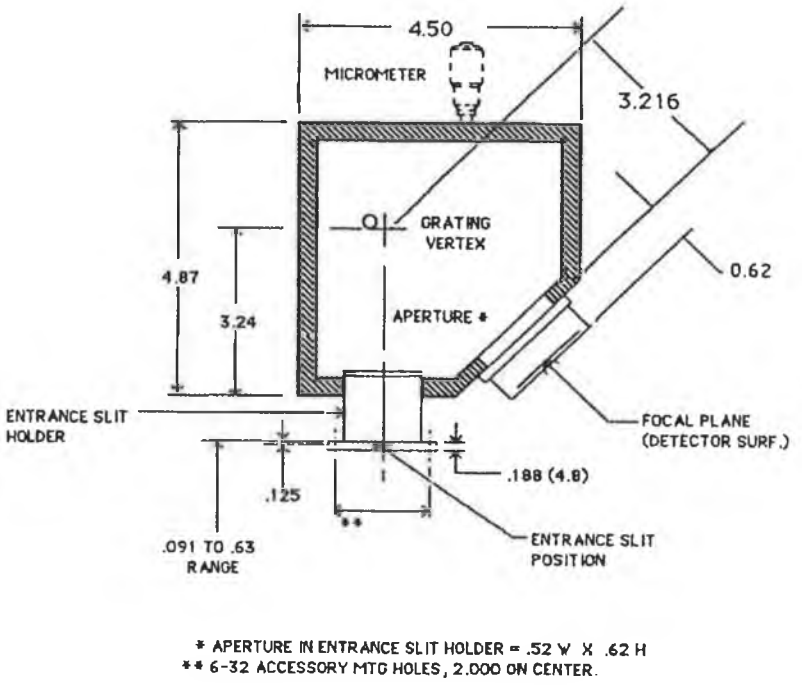

Figure 2.5 A diagram of the American Holographic 100S spectrograph.

The wavelength is driven by means of a locking micrometer. This micrometer, unlike in the Multispec spectrograph, was not wavelength calibrated. This means that the system can be calibrated for a certain wavelength range and the micrometer setting noted, but if a new wavelength range is required the system must be re-calibrated for the new range. This is time consuming but because of the repeatability of the micrometer, previously calibrated wavelength ranges can be quickly selected by going to the noted micrometer reading. In Section 2.5.5 the procedure for calibrating the spectrograph is described.

The entrance slit of the spectrograph can be vertically adjusted so as the spectrum can be centred vertically at the detector plane. The spectrograph has external focusing adjustment, achieved by in-out movement of the barrel assembly onto which the entrance slit is mounted. This in-out adjustment in effect varies the distance between the entrance slit and the grating. This focusing is necessary because best focus over the entire spectral region involves a compromise, since the focal surface even for "flat field" gratings has a residual curvature. Thus the location of the

focal plane must be adjusted to minimise focus variations over the spectral range of interest.

The CCD type used by the OMA4 detector, model 1530P-1024S, is a Thomson CSF THX-31159A front-illuminated 4 phased CCD. The spectral range of the CCD is 400-1100nm. This is defined by the photosensitive material type used, which in this case is also silicon, but without the advantage of enhanced UV response.

The sensor area is 1024 by 256 pixels with each pixel being 19μm by 19μm in size. Like the InstaspecIV CCD, this CCD is designed with spectroscopy in mind because the readout register is along the long, *i.e.* the 1024 element, axis.

The CCD uses a 3 stage Peltier cooler with a temperature feedback. The heat generated by the Peltier device can be extracted by using either water or ethylene glycol. A temperature range of -70^0C to + 10^0C is attainable using water to dissipate the heat whereas if ethylene glycol is used a temperature range of -80^0C to + 10^0C is possible.

The typical noise of each pixel is 1 to 1.2 counts, where a count is equal to 4 photoelectrons. The well capacity is of the order of 1.2×10^6 electrons (roughly 300,000 counts). Consequently, optimum compatibility between the detector and the ADC is achieved using an 18 bit ADC (262,144 levels), giving a maximum dynamic range for the system of 262,144 : 1. The rear of the detector housing contains many electrical connections and a detailed explanation of the purpose of each connection is given in the relevant manual [3]. The only connections of interest to this project were TRIG IN and the power connection. The former was used to define the moment in time when a spectrum would be captured and the latter powered up the CCD and all the electronics in the CCD housing. Power was supplied by the OMA4 powerblock, model 1533. The TRIG IN connection contains an opto-isolator circuit, which is used to filter noise and prevent ground loops, as discussed in Section 2.5.2.

This CCD, like the InstaspecIV, is computer controlled via a controller card, model 1564, and the OMA4-SPEC-4000 applications software. This software facilitates the capture and signal processing of spectra. It is also used to set such CCD's parameters as the exposure time, the CCD temperature and the number of rows to be binned. The computer procedure used to co-ordinate the wafer mapping system is described in the Section 2.6.

The link between the controller card and the CCD is made via optical fibres. This arrangement is used instead of an electrical connection because it is less prone to electrical pick up.

2.5.4 OMA4/100S Spectrograph Alignment

The OMA4 CCD had to be aligned with the spectrograph. There are two concerns to address when aligning:

1. Positioning of the detector's focal plane so that it corresponds with the spectrographs focal plane. This is called In/Out alignment.
2. Rotating the detector so that its resolution elements are parallel with the signal output of the spectrograph. This is called Rotational alignment.

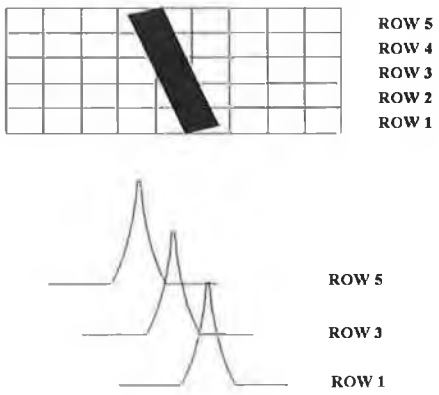

Figure 2.6 Rotational misalignment.

The in-out alignment involves imaging a spectral source on the CCD and adjusting the spectrograph's external focusing, mentioned in Section 2.5.3, until the spectral lines, as viewed on the computer monitor, become clearly defined and are at their maximum intensity.

The rotational alignment involves setting up the CCD so that each of the 256 rows are viewed separately, *i.e.* none of the rows are binned. The reason for this is that it is not possible to detect rotational alignment by looking at a single row because the spectral line is of comparable width to a pixel in the CCD array. Select at least 2 rows, well separated, that clearly show a variation in the pixel position of the spectral

line's peak with respect to the row number. This variation in the pixel position is due to the spectral line being angled on the CCD array, as shown in Figure 2.6. Rotate the CCD with respect to the spectrograph until the spectral line's peak appears at the same position in the selected rows, as shown in Figure 2.7.

A more detailed account of how to perform both of these alignments is given in the CCD manual [3].

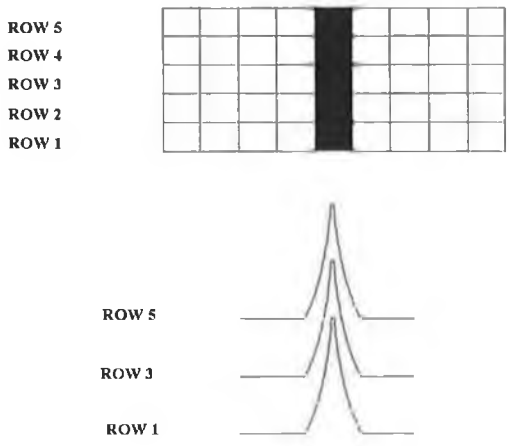

Figure 2.7 Correct rotational alignment.

An example of a type of spectral source that could be used when aligning is a low pressure mercury lamp.

2.5.5 Wavelength Calibration of the OMA4/100S Spectrograph

In Section 2.5.3 it was stated that there was no known relationship between the movement of the wavelength drive and the shifting of the central wavelength viewed by the CCD, in contrast to the InstaspecIV system. Thus the system has to be calibrated every time a new wavelength range is required.

To calibrate the system for a certain wavelength range a light source which has distinct peaks within this region, for which the wavelength values are known, is needed. The light source is aligned with the entrance slit of the spectrograph and a spectrum is captured. Then it is a simple process of assigning the wavelength values to the peaks and letting the software calculate the wavelength range being viewed, a more detailed account of this calibration is given in reference [6].

There are three degrees of fit available to the user, *i.e.* linear, square or cubic, between the pixel location and the spectral line. The linear degree of fit is used where there is a linear or near linear relationship between the wavelength units and the pixel spacing. It finds the best fit straight line between two or more data points using a linear equation. The square degree of fit finds the best fit curve between three or more data points using a second order equation. This is more accurate than the linear fit near the selected calibration points but due to its curve nature tends to become less accurate at points away from the calibration points. Thus a greater spread of data calibration points is needed for the square fit. The cubic degree of fit is recommended where there is a clearly non-linear relationship between the wavelength and the pixel location. It uses a third order equation to select the best fit curve between four or more data points. No more than fifteen data points can be used in calibrating the system.

When the calibration is finished the calibration spectrum can be saved as a file to the hard disk. This saved file contains the spectrum and the calibration coefficients. Thus this calibration can be recalled and used in the future by loading the file and extracting the coefficients from the file, using the commands available in the OMA4 software package, see the OMA4 manual [6].

In summary, the system can be calibrated for any wavelength range and by noting the micrometer setting these calibrated wavelength ranges can be recalled any time in the future.

2.6 Computer Interfacing

The computer interfacing involved writing computer programs that would co-ordinate and automate the wafer mapping system. Two computer programs were necessary, one to control the xy translation table and the other to control the CCD. Even though these are two independent programs they are linked by the fact that the CCD waits for a pulse from the xy translation table controller (the NF90) before it will acquire data. Thus the xy translation table is the master and the CCD is the slave. Figure 2.8 is a flow chart which shows the basic sequence of events in the automation of the system.

As stated in Section 2.2, the code used to control the xy translation table is a specialised code. This code has to be incorporated into a more traditional programming language, *e.g.* Quickbasic or Pascal, so that it can then be downloaded, as a string of characters, to the NF90 via a RS-232C cable. The code for this program is given in Appendix A. For a detailed explanation of what each command means see [7].

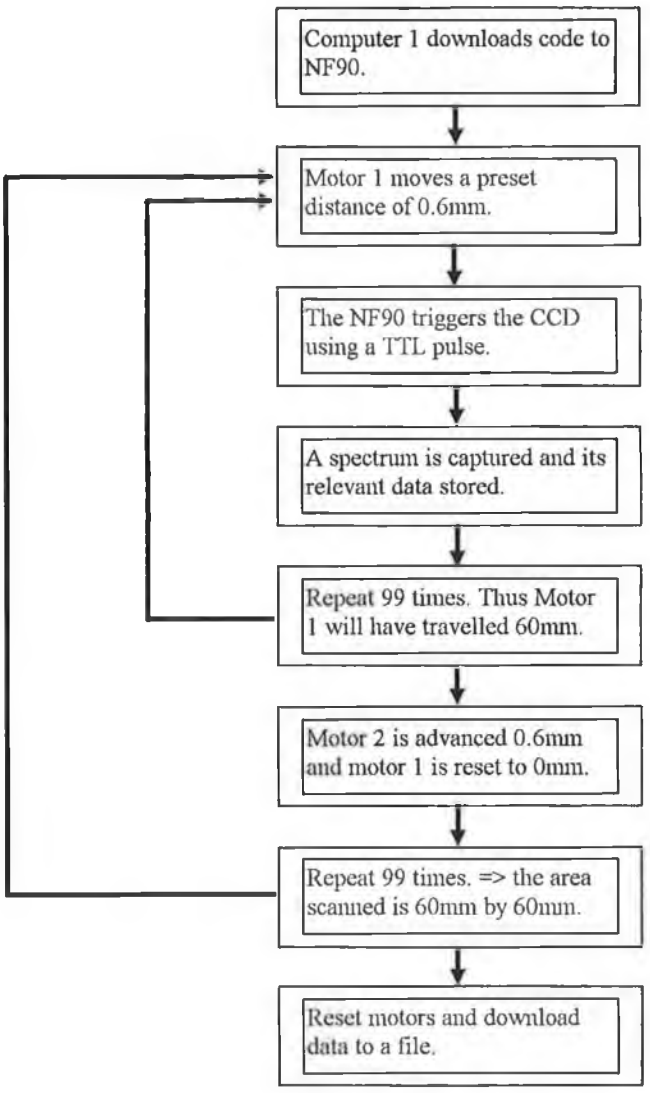

Notes on flow chart:

1) The motor step-size is user defined and can have a range of values. The value of 0.6mm given in the flow chart was just used as an example.

2) Motor 1 accounts for motion across the wafer and motor 2 accounts for motion down the wafer.

3) The relevant data taken from a spectrum, for this project, are the peak intensity and the peak wavelength.

Figure 2.8 A flow chart of the computer control of the wafer mapper.

A second computer was used to control the operation of the CCD, using the supplied software package. This package enables the user to set all the necessary parameters, such as exposure time and the amount of binning to be performed, for the

CCD to operate in real time mode. It also facilitates the writing of custom programs that will allow the user to define when a spectrum is to be acquired and what data processing is to be performed on this spectrum. Both CCD systems had their own programming language. The InstaspecIV used a customised Basic language and the OMA4 used a customised Pascal language. Even though the languages were different the basic steps involved in the automation of the CCD were the same. The flow chart shown in Figure 2.9 shows the sequence of these steps. This flow chart is a more detailed description of what happens in block four of the previous flow chart. The actual programs that were written to control both CCD systems are given in Appendix A.

To operate the OMA4 CCD another program has to be run. This program is called a data acquisition sequence (DAS) and it determines the order of events that are to occur when data is acquired. It is written in a lower level computer language. The DAS program has to be called by the Pascal type program during a scan. An example DAS program, as supplied by EG&G PARC, was used in this project.

2.7 Conclusions

The wafer mapping unit was successfully implemented, as shown in Figure 2.1, using both detector/spectrograph systems and maps of the peak wavelength and the peak intensity were recorded at various temperatures, for different wafers, some of which are shown in the next chapter.

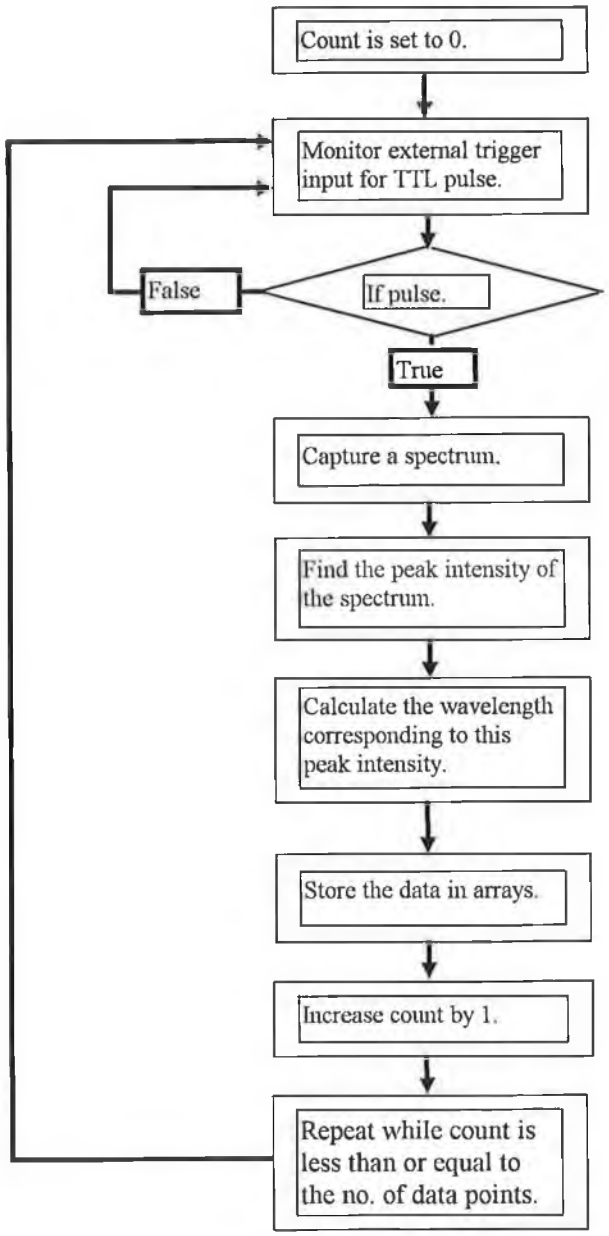

Notes on flow chart:

1) The no. of data points is the total number of points on the wafer that are scanned.

2) It is possible to measure parameters other than the peak intensity and the peak wavelength, such as the FWHM and λ_+.

3) It is also possible to monitor more than one peak in the spectrum at a time.

Figure 2.9 A flow chart of the CCD's computer control.

References

1. Melles Griot, *Optics Guide 5*, 1990.
2. Janis Research Company Inc. (USA), *Operating Instructions For The Janis DT Series Research Dewar.*
3. EG&G Princeton Applied Research, *OMA-Vision CCD Detector (TE-Cooled) User's Manual*, 1991.
4. M. Catney (Andor Technology), *Private Communication.*
5. Oriel Corporation, *Oriel Catalogue*, **Vol. II**, 1994.
6. EG&G Princeton Applied Research, *OMA Spec 4000 Applications Software Manual*, 1991-1992.
7. Velmex Inc. (USA), *NF90 Series Users Guide*, 1992.

Chapter 3

Results

3.0 Introduction

This chapter contains maps and spectra of three different semiconductor wafers. These maps detail information about variations in peak intensity and peak wavelength across the wafer. Two of the wafers were scanned using the InstaspecIV system and the other wafer was scanned using the OMA4 system.

3.1 Wafer Mapper Resolution

The minimum distance possible between two successive scanned points on a wafer is the resolution being discussed in this section. Even though the translation table has a minimum step size of 5μm, the definitive resolution of the system is closer to 100μm. This is determined by the optics being used to focus the laser on the wafer and the fact that the carriers generated in the illuminated area can easily diffuse over distances of the order of several microns, as reviewed in [1].

If a 50mm wafer was to be mapped at this resolution (100μm) at least 270,400 points would have to be scanned and considering that it takes four hours for a 10,000 point scan, the length of time necessary for a 270,400 point scan would make such a scan impractical, especially when working at liquid helium temperatures. The reason for the large number of data points is that in order to scan a wafer of 50mm in diameter it is necessary, in the system we have developed, to scan a square with sides greater than 50mm, so as the whole wafer will be mapped. Therefore if a scan size of 52mm by 52mm is to be performed with a step size of 100μm the number of data points necessary works out as 270,400.

Although the factors above define the resolution of the wafer mapping system, the time taken to scan a whole wafer determines the practical resolution. There are improvements that can be made to the system, discussed in Section 4.1, which will

reduce the scan time and therefore bring the practical limitations of the system closer to the theoretical limits.

The minimum step size used to date is 600μm, as anything lower would take too long.

3.2 Maps and Spectra

This section consists of two subsections. The first subsection deals with the maps and spectra obtained from scanning two different wafers using the InstaspecIV system and the other deals with the maps and spectra obtained from scanning a single wafer using the OMA4 system.

3.2.1 InstaspecIV Results

The first wafer mapped consisted of a GaAs epilayer on a semi-insulating GaAs substrate. This wafer will be referred to as wafer A from here on. A spectrum showing the PL line of interest is given in Figure 3.1. This line is centred at ~850nm. It has a very broad peak with a full width at half maximum (FWHM) equal to ~58nm. The spectrum was taken with an exposure time of 10ms, the CCD cooled to -20^0 C, the laser output power at 160mW and the wafer at room temperature (~290K).

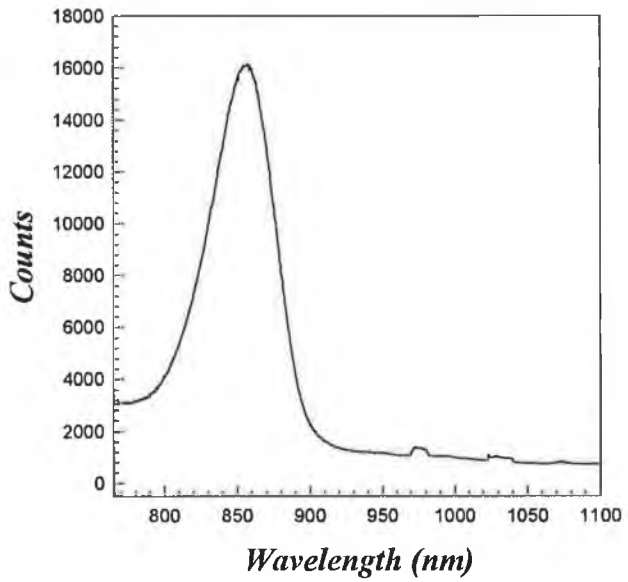

Figure 3.1 A typical PL spectrum of wafer A recorded at room temperature.

The background signal that appears at the lower end of the wavelength range may be due to the weak broadband luminescence from the outermost window in the cryostat, which is made from sapphire.

Spectra (such as that shown in Figure 3.1) were recorded at 0.6mm intervals over the wafer and the maps produced will now be described. In the course of producing these wafer maps the possibility of geometrical factors influencing the data was examined. To do this two maps were recorded for the second of which only the wafer orientation in the optical system was changed (a 90^0 rotation).

The map shown in Figure 3.2 details the variation found in the peak wavelength across wafer A. There is good uniformity in the map, with a spread of only 7nm observed (each colour corresponds to an interval of 1nm). Among the possible causes for the wavelength variations that occur is changes in the n-type doping levels in the epilayer. The map in Figure 3.3 is that produced for the wafer rotated through 90^0.

The reproducibility of the system and the lack of dependence on wafer orientation is displayed well in these maps. For example, there is a dark blue ridge on the curve of the top left quadrant of the wafer in Figure 3.2 which is positioned at the bottom left quadrant after the 90^0 rotation, as can be seen in Figure 3.3. Slight variations do occur between these two maps, for example there is a greater spread of the colour green/yellow on the second map. The PL line has a broad peak, thus any noise on the signal could affect the position of the peak wavelength by 1nm or less. Also the software used to obtain a colour printout of a wafer map rounds the data off to the nearest integer. Therefore this combination of rounding off the data to the nearest integer and the broad nature of the peak of the PL line could result in a different colour to be displayed at that point on the wafer map and thus cause the slight variations noticed between these two maps. Consequently, one has to be very careful when trying to interpret the information from the colour plots.

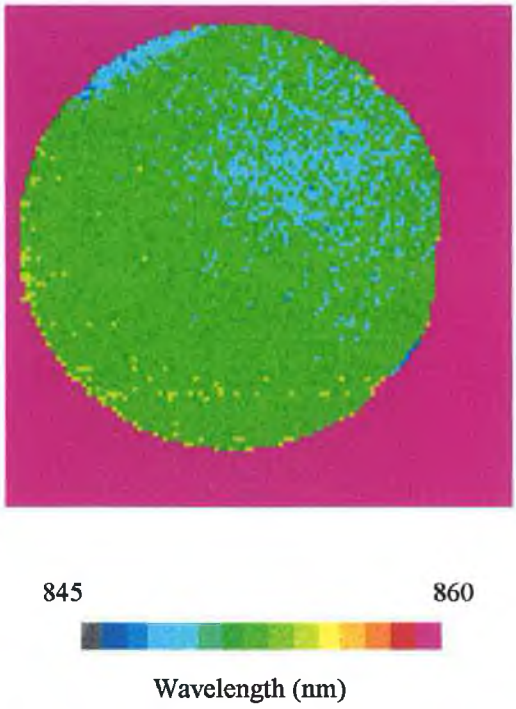

Figure 3.2 A peak wavelength map of wafer A recorded at room temperature.

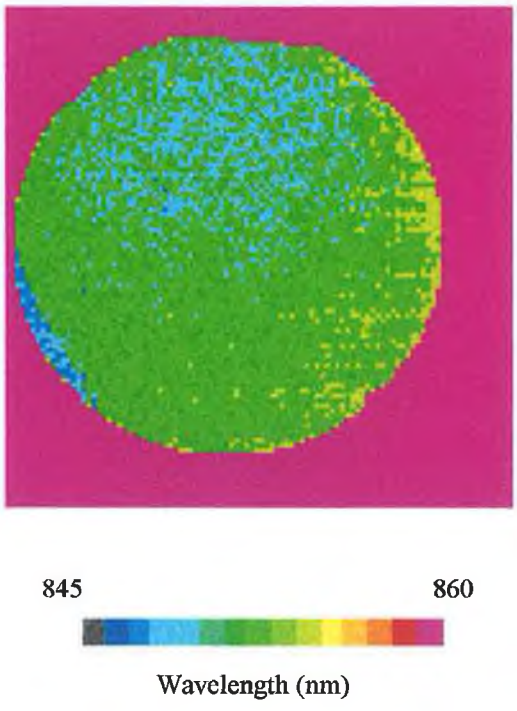

Figure 3.3 A peak wavelength map of the same wafer shown in Figure 3.2 but in this case the wafer has been rotated through 90^0 in an anticlockwise direction.

The peak intensity map shown in Figure 3.4, recorded at the same time as the peak wavelength map shown in Figure 3.2, shows a spread in intensity from 8000 to 17000 counts. Each colour corresponds to a peak intensity range of 600 counts. The peak intensity map does not show the uniformity that was present in the wavelength map. These large changes in peak intensity are quite possibly due to variations in defect densities [2]. There are some correlations between the peak intensity map and the corresponding peak wavelength map; for example the orange and red region (top left) on the peak intensity map has roughly the same shape and location as a blue region in the wavelength map. It is likely that there is a common origin to both these effects, but the study of such details is outside the scope of this work.

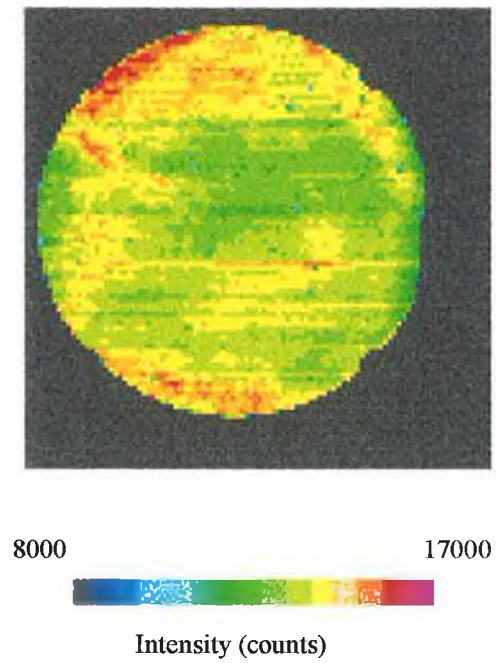

Figure 3.4 A peak intensity map of wafer A recorded at room temperature.

The laser was prone to intermittent changes in the output power. These fluctuations did not affect the peak wavelength maps but caused "blocky" structures to appear on the peak intensity maps. Figure 3.5 shows an intensity map of wafer A which has been rotated through 90^0 in an anticlockwise direction from that shown in Figure 3.4. The aforementioned blocky structure can be observed to a small degree in this map. A more pronounced instance of this effect is shown in the intensity map, Figure 3.6, of wafer C which is described in Section 3.2.2. A solution to this problem is suggested in Chapter 4.

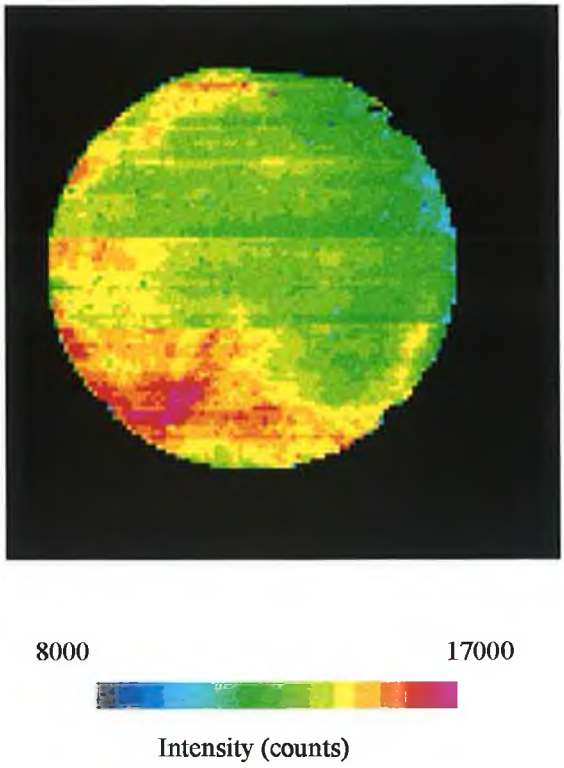

Figure 3.5 A peak intensity map of the same wafer shown in Figure 3.4 but rotated through 90^0 in the anticlockwise direction.

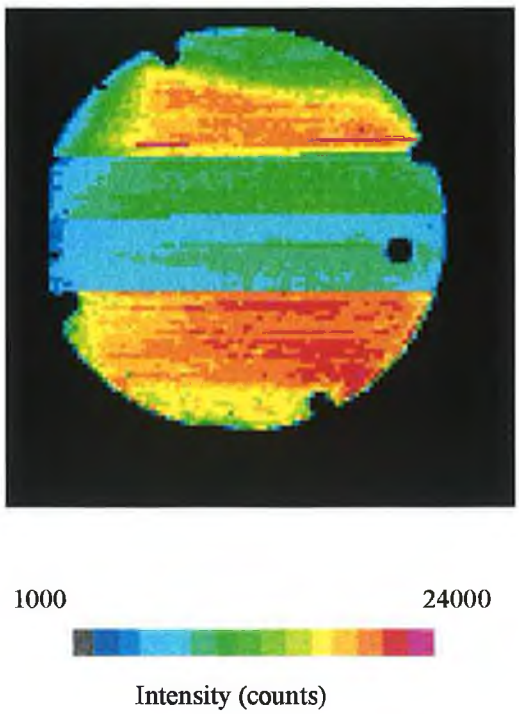

Figure 3.6 A peak intensity map of wafer C recorded at room temperature showing distinct blocky structures caused by laser output fluctuations.

The second wafer scanned was a superlattice structure grown using metal-organic chemical vapour deposition (MOCVD) on a GaAs substrate. The superlattice structure consisted of a series of 20 latticed-matched well and barrier layers each of nominal thickness 2nm. The well material was InGaP while the barriers consisted of AlInP. A capping layer of InGaP, of thickness 50nm, was grown over the superlattice. (Appendix B contains a schematic diagram detailing the structure). This wafer will be referred to as wafer B from here on.

Figure 3.7 shows a PL spectrum recorded at a point on wafer B. The spectrum was recorded at liquid nitrogen temperature (77K), with an exposure time of 25ms and a laser output power of 65mW. There are three PL lines present. Line 1 is centred at ~605nm and is due to recombination within the superlattice. Line 2 is centred at ~645nm and is due to the capping layer. Line 3 is centred at ~820nm and is due to the GaAs substrate. The interpretation of PL data from similar structures is discussed in detail by Lambkin *et al* [3].

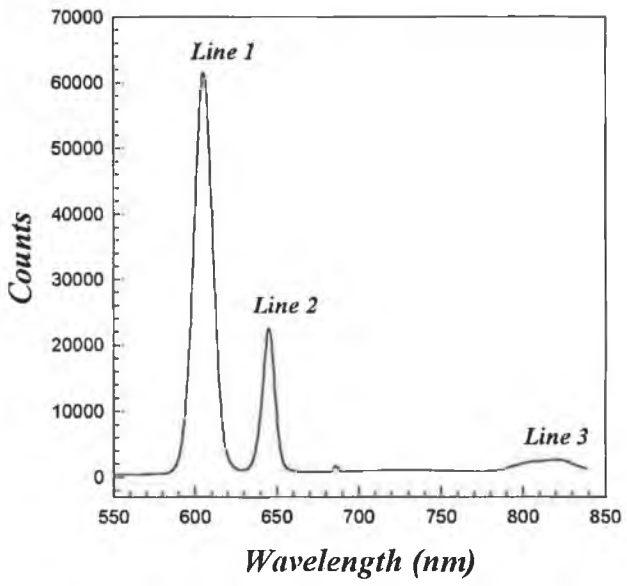

Figure 3.7 A typical PL spectrum of wafer B recorded at liquid nitrogen temperature.

A PL spectrum was also recorded at liquid helium temperature (4.2K) with an exposure time of 25ms and a laser output power of 50mW, see Figure 3.8. As with

Spectra were recorded at different points on the wafer at liquid helium temperatures. In Figure 3.9 two of these spectra are shown on the one graph. The peak wavelength shifts are clearly observable from this graph.

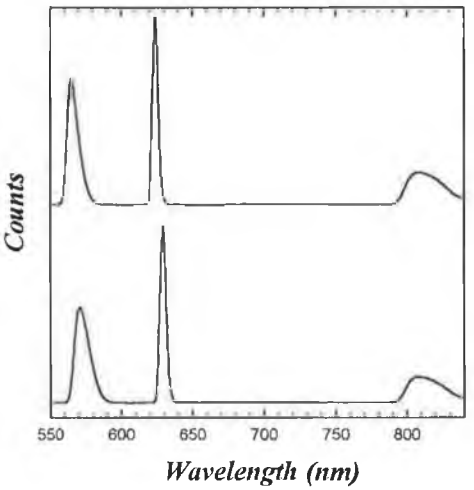

Figure 3.9 A graph of PL spectra from 2 different points on wafer B recorded at liquid helium temperature.

Wafer B was scanned at 4.2K, with a CCD exposure time of 25ms and a laser output power of 50mW. The distance between successive scanned points on the wafer was 0.6mm. The information collected at each of these points was the peak wavelength and peak intensity for lines 1 & 2. Figures 3.10 and 3.11 show the peak wavelength maps for lines 1 & 2 respectively. The peak wavelength drops gradually in value in going from the top to the bottom of the wafer, in both maps. The variations in the peak wavelength for a superlattice structure are normally due to either variations in the alloy composition or well width, but in this case it is more than likely that it is due to the former because of the similarity between the map for the superlattice and the map for the capping layer. The reason for the compositional changes is thought to be due to the details of the gas flow in the MOCVD growth chamber[4]. Each colour in these maps corresponds to a wavelength range of 3nm. This is equal to roughly 75% of the FWHM for line 1 and roughly 60% of the FWHM for line 2. Thus in the map for the superlattice layers (line 1) a spread in wavelength of 39nm across the wafer was observed. The map which deals with the capping layer has a spread in wavelength of 33nm across the wafer.

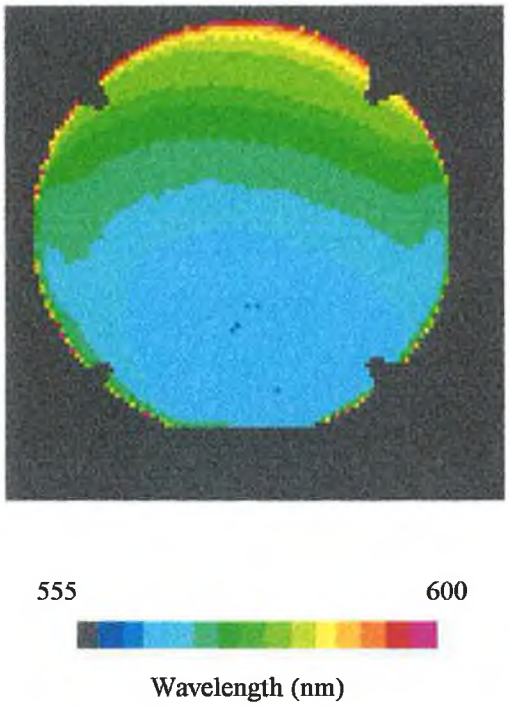

Figure 3.10 A peak wavelength map of the superlattice (line 1) in wafer B recorded at liquid helium temperature.

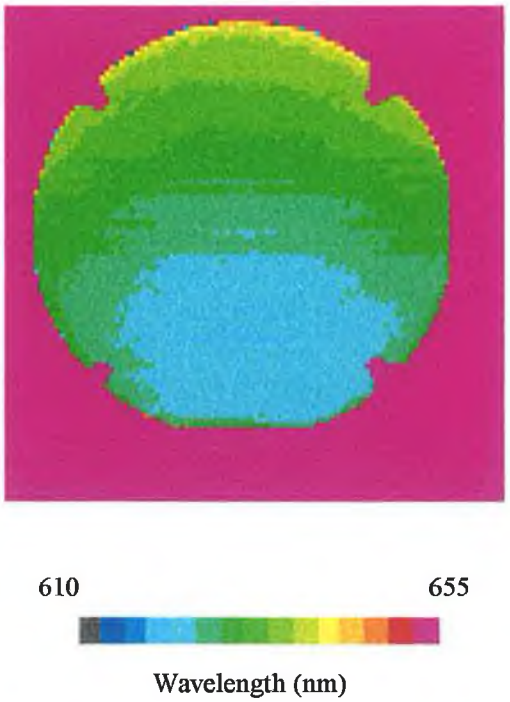

Figure 3.11 A peak wavelength map of the capping layer (line 2) in wafer B recorded at liquid helium temperature.

In these two maps there appears to be four pieces missing from the wafers. These missing pieces are a result of small Teflon protrusions on the sample holder blocking the laser from striking the wafer. These missing sections appear on all of the following maps and to a lesser extent on the previous maps.

No suitable peak intensity maps were recorded as they were all affected by laser output power fluctuations.

3.2.2 OMA4 Results

The wafer scanned using this detector/spectrograph combination consisted of an InGaAs quantum-well structure grown on a Si doped GaAs substrate. See Appendix B for a schematic diagram detailing the different layers of this wafer. From here on this wafer will be referred to as wafer C.

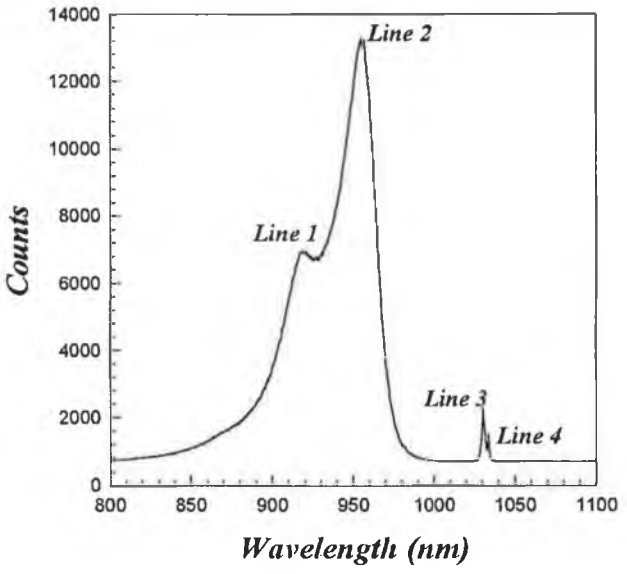

Figure 3.12 A typical PL spectrum of wafer C recorded at room temperature.

A room temperature PL spectrum of wafer C is given in Figure 3.12. The CCD was cooled to 0^0 C and set to an exposure time of 2ms. The laser output power was 120mW. There are four peaks in this spectrum. Lines 3 & 4 are centred at wavelengths 1030nm & 1033nm respectively and are second order laser lines. Line 1, centred at ~918nm, is due to transitions from a thermalising excited state of the

quantum-well. Line 2, centred at ~955nm, is due to emission from the lowest excited state of the quantum-well.

Wafer C was scanned at room temperature, with a laser output power of 80mW and an exposure time of 0.5ms. The distance between each successive scanned point was 0.6mm. The line that was monitored for this scan was line 2. The peak wavelength map which resulted from this scan is shown in Figure 3.13. There is a definite variation in peak wavelength across the wafer. The possible reasons for this variation was discussed in Chapter 1. In brief, for the growth of a quantum-well structure such as in this sample, the peak wavelength observed depends on the growth temperature, alloy composition and well width. For wafers of 50mm diameter, achieving high uniformity for all three parameters is difficult. For example, in some cases fine structure has been observed in the luminescence spectra due to variations as small as a monolayer in quantum-well width [5]. Similarly, a composition change of InGaAs from a Ga : As ratio of 1 : 1 to the more commonly used 0.47 : 0.53 (for lattice matching to InP substrate wafers) produce a shift in the bandgap which corresponds to a wavelength shift of 48.7nm. In the optimisation of a growth process, wafer maps such as that illustrated in Figure 3.13 are recorded for a variety of growth conditions (*e.g.* temperature, gas flow rate, gas mixture). The scope of the data obtained, covering peak wavelength, intensity and uniformity, is especially helpful in establishing optimum growth conditions.

In going from the top of the wafer to the bottom the peak wavelength shows an overall increase in its value. Each colour on the map corresponds to a wavelength range of 2nm. Thus, in going from the top of the wafer to the bottom there is a change in wavelength of roughly 8nm. The central edge of the left handside of the map and, to a lesser extent, the central edge of the right handside are the areas where the greatest wavelength variations occur. There are at least six colours represented here. However, it must be noted that for the most part only three colours are predominant across the whole wafer.

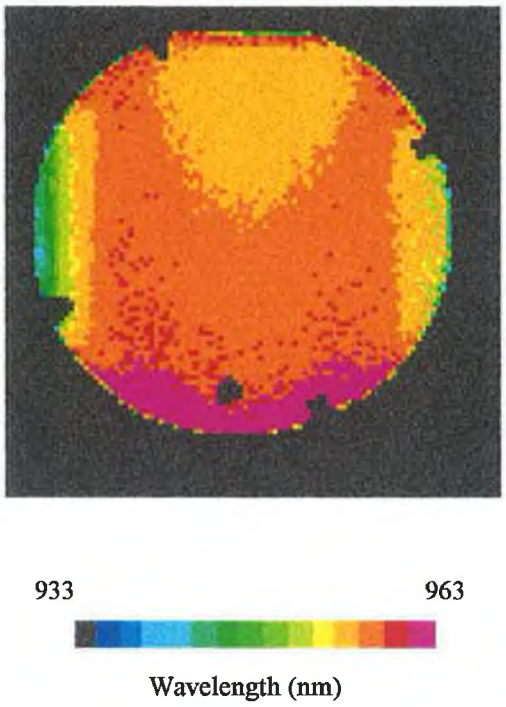

Figure 3.13 A peak wavelength map of the quantum-well (line 2) in wafer C recorded at room temperature.

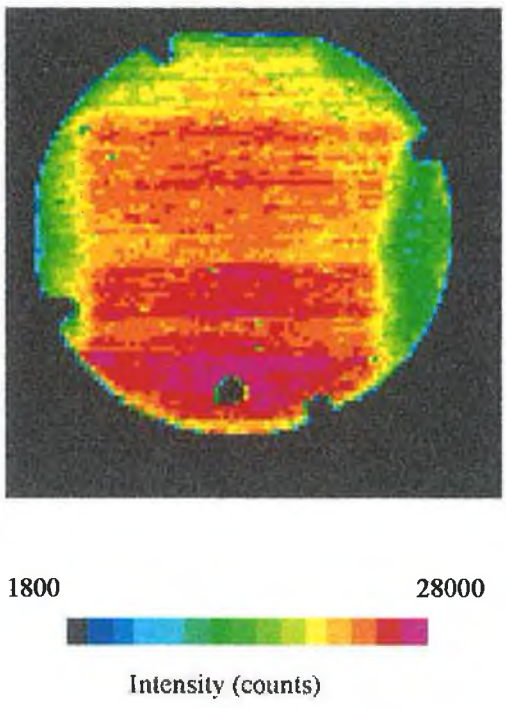

Figure 3.14 A peak intensity map of the quantum-well (line 2) in wafer C recorded at room temperature.

The black region located at the bottom of the peak wavelength map also appears in the peak intensity map (see Figure 3.14). There is little or no PL emission from this area of the wafer, the intensity at any point in this region being roughly 2000 counts, and any signal that appears here is due to background light and noise. Thus, there is a major defect present at this point on the wafer. The cause of this defect is of no importance to this work and is therefore not explored any further.

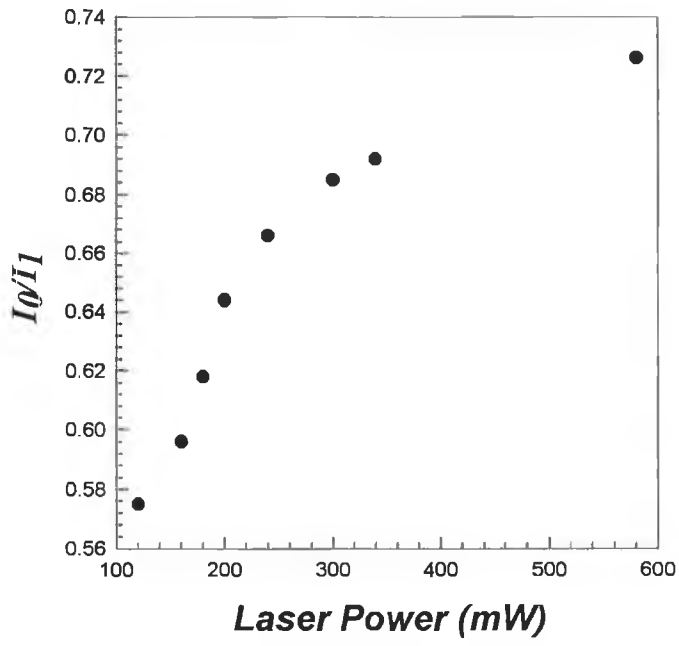

Figure 3.15 A graph of the ratio of the peak intensities of line 1 (I_0) and line 2 (I_1) versus the laser output power.

Line 1 in the spectrum displayed in Figure 3.12 is due to thermalisation, as previously stated. Proof of this is given by the fact that the line does not appear in spectra recorded at liquid nitrogen temperatures (see Figure 3.16). This thermalisation effect itself is due to the heating action caused by the focused laser spot on the sample. To show that this is the case, the ratio of the peak intensities of the two lines was calculated for a number of different laser output power values. A graph of this data is shown in Figure 3.15. It is clear from the graph that the ratio of the peak intensities increases with higher laser power values. Thus for a single increase in the value of the laser output power line 1 shows a greater increases in intensity than line

2. Therefore the laser output power has a greater influence on the peak intensity of line 1 and this is due to the thermalisation being caused by the focused laser spot heating the sample. The degree to which the focused laser beam raises the temperature of the wafer, for the laser output powers used in Figure 3.15, is discussed in Section 3.3.

The spectrum shown in Figure 3.16 was recorded with a CCD exposure time of 0.5ms and the CCD cooled to -20^0 C. The laser output power was 80mW. Only one line is present in the spectrum, centred at ~889nm. This line is due to PL emission from the quantum-well. At room temperature the PL line was centred at ~955nm. Thus by reducing the sample's temperature to 77K a wavelength shift of ~66nm was experienced. Also the PL line has become sharper. The full width at half maximum at 77K is ~9nm whereas at room temperature it is ~35nm.

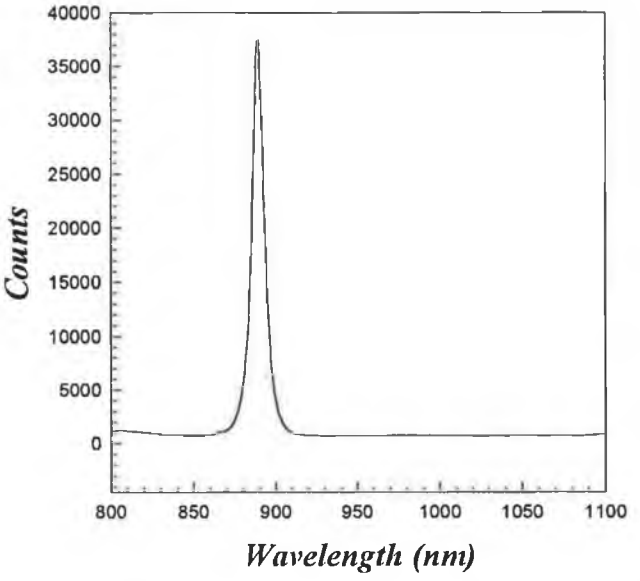

Figure 3.16 A typical PL spectrum of wafer C recorded at liquid nitrogen temperature.

A second spectrum was recorded at 77K with the same CCD and laser settings but at a different point on the wafer. This spectrum is shown in Figure 3.17 together with the spectrum of Figure 3.16. It is clear that the peak wavelength value changes in going from the first point on wafer C to the second point. To quantify this statement,

the peak is centred at ~906nm in the top spectrum whereas it is centred at ~889nm in the bottom spectrum. Thus the peak wavelength value experiences a shift in value of ~7nm in going from the first point to the second.

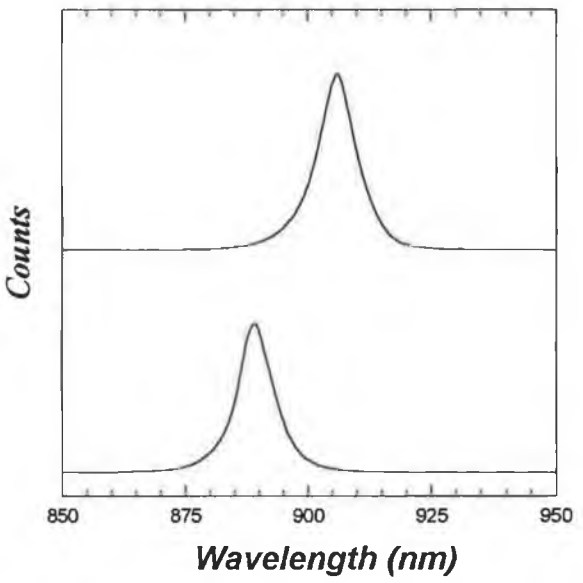

Figure 3.17 A graph of PL spectra from 2 different points on wafer C recorded at liquid nitrogen temperature.

Wafer C was scanned at 77K so that the extent of these variations in peak wavelength across the whole wafer could be observed. The distance between each successive scanned point was 0.6mm. The CCD and laser settings for this scan were the same as they were for the recording of the previously shown spectra. The peak wavelength map that resulted from this scan is shown in Figure 3.18. Each colour corresponds to a wavelength range of 2nm. For the most part there are only three colours represented in the map and they are green/yellow, yellow and orange. Thus the peak wavelength is uniform in these regions to within 6nm. The places where the most variation occurs are the central edges of the right and left handsides of the map, with the left handside showing the greatest variation with six colours being displayed in this region. This was also the case for the wavelength maps recorded at room temperature.

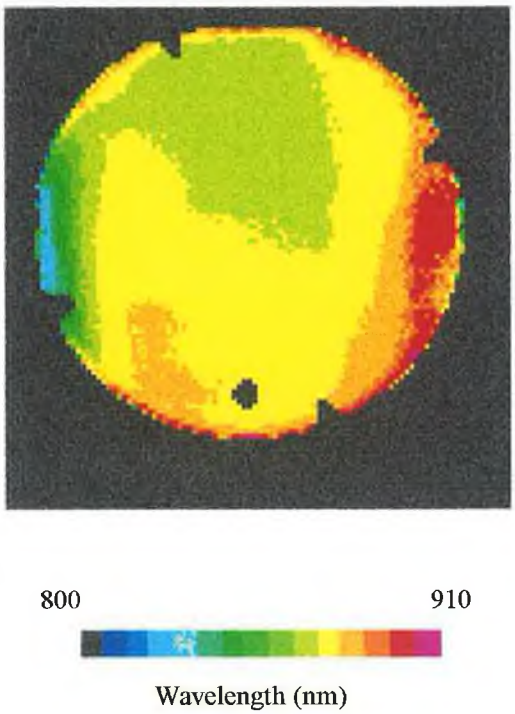

Figure 3.18 A peak wavelength map of the quantum-well in wafer C recorded at liquid nitrogen temperatures.

3.3 The Heating Effect of The Focused Laser Beam at Room Temperature.

As previously stated line 1 in Figure 3.12 is due to transitions from a thermalising excited state of the quantum-well. As indicated earlier the intensity of this line relative to line 2 changes with laser power, the change being due to the heating of the sample by the focused laser beam heating the sample. In this section the temperature increase experienced by the sample is calculated and discussed.

The ratio of the intensities of two thermalising lines is given by equation 3.1,

$$I_0/I_1 = A\exp\left(-\Delta E/kT\right) \qquad (3.1)$$

where A is the intrinsic intensity ratio in the absence of any temperature effects, ΔE is the energy difference between the two lines, k is Boltzmann's constant and T is the temperature of the sample.

It is possible to estimate the value of I_0/I_1 when the laser output power is zero (equivalent to having no heating effect) by extrapolating the graph in Figure 3.15 to zero laser power. This extrapolation gives a limiting value of ~0.5. Line 1 (I_0) is centred at ~918nm and line 2 (I_1) is centred at ~955nm, thus the corresponding ΔE

between these two lines is ~50meV. Inserting the values for I_0/I_1 and ΔE just calculated and a sample temperature (T) of 290K (room temperature) into equation 3.1 yields a value for A of ~4.

The actual temperature of the sample can now be calculated for each of the laser powers shown in Figure 3.15, using equation 3.1 and the known values ΔE, **A** and I_0/I_1.

The data that resulted was then displayed as a graph (see Figure 3.19) of the number of degrees Kelvin the sample temperature is above 290K versus the laser power. This graph shows that the temperature of the sample, at the point on which the laser is focused, initially increases roughly linearly with increasing laser power up to 340K and then it begins to level off. The effect is quite significant, even at the lowest laser powers used, and for a detailed investigation of the spectra (as opposed to spatial variations) this heating effect would need to be taken into account.

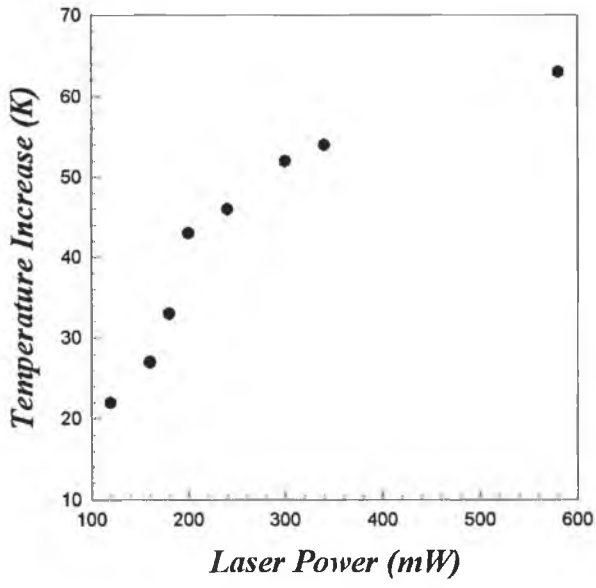

Figure 3.19 A graph of the temperature increase of the sample versus the laser output power.

3.4 Conclusions

This chapter showed that the system worked successfully for both detector/spectrograph configurations. For the three wafers scanned peak wavelength and peak intensity maps were recorded which showed variations which were typical of those reported in other studies of similar structures produced using the same growth procedures [6-8]. The peak intensity maps give a measure of the wafer material's purity and lattice quality and the peak wavelength maps can, among other things, be used to determine the lasing wavelength of lasers built from these wafers [9].

The ability of the system to work at cryogenic temperatures was also successfully demonstrated as some of the maps were recorded at liquid nitrogen and liquid helium temperatures. As with all new systems there are problems which have yet to be solved, such as laser output power fluctuations and the length of time taken to perform a wafer scan. Possible solutions to these problems are discussed in the next chapter.

References

1. P.M. Fauchet "Applied Optical Diagnostics of Semiconductors" *Proceedings of The IEEE,* **Vol. 80**, No 3, pp. 420-435, March 1992.
2. G.E. Carver, M.L. Gray, J. Levkoff, B.W. Miller and B.S. Phatak, "Non-Destructive Optical Technique for Characterizing Semiconductor Materials and Devices" *AT&T Technical Journal*, pp. 66-76, March/April 1994.
3. J.D. Lambkin, A.P. Morrison, L. Considine, G.M. O'Connor, C.J. McDonagh, E. Daly and T.J. Glynn "Energy band structure of type I and type II InGaP/InAlP short period superlattices" *Proceedings of the International Conference on the Physics of Semiconductors*, World Scientific Publishing Company, Singapore, 1995.
4. J.D. Lambkin (NMRC, Cork), *Private Communication.*
5. D.C. Reynolds *et al* "Determination of interface quality of GaAs-GaAlAs multi-quantum well structures using photoluminescence spectroscopy" *Applied Physics Letters*, **Vol. 46**, No. 1, pp. 51-53, January 1985.
6. D.J. As, S. Korf, Z.M. Wang, J. Windscheif, KH. Bachem and W. Jantz "Low-Temperature Photoluminescence topography of MOCVD-Grown InGaP, AlGaAs and AlGaAs/GaAs Single Quantum Wells" *Semiconductor Science and Technology*, **Vol. 7**, Iss. 1A, pp. A27-A31, January 1992.
7. C J Miner "Non-destructive, whole wafer assessment of optoelectronic epitaxial materials" *Semiconductor Science and Technology*, **Vol. 7**, Iss. 1A, pp. A10-A15, January 1992.
8. C.J.L. Moore and C.J. Miner "A Spatially Resolved Spectrally Resolved Photoluminescence Mapping System" *Journal of Crystal Growth*, **Vol. 103**, pp. 21-27, 1990.
9. J. Hennessy, C. Miner and C. Moore "Photoluminescence Mapping in Inspection and Process Control" *Photonics Spectra*, pp. 91-96, April 1990.

Chapter 4

Conclusion

4.0 Summary of Work

The objective of this project was to construct a system that facilitated the spatial and spectral characterisation of semiconductor wafers at various cryogenic temperatures using PL as the characterisation technique. The various maps displayed in Chapter 3 are a clear indication of the success of the PL wafer mapping system developed. These maps show spatial variations in the peak wavelength and peak intensity values for three separate wafers. The peak wavelength variations are possibly caused by changes in the alloy composition of the epitaxial layer and/or deviations in the width of the quantum-well. The peak intensity maps yield information on the extent and spatial distribution of defects in the wafer.

The use of a CCD/spectrograph is central to this system as it enabled spectra to be recorded and the various parameters to be calculated from the spectra in real time. Two separate CCD/spectrograph units were used in the system, each with particular advantages and disadvantages, some of which are listed in Table 4.1. The InstaspecIV is a more user friendly compact single system than the OMA/American Holographic combined system. Consequently, it seems like the obvious choice for the wafer mapping unit except that it crashed intermittently when used in external trigger mode. This is not acceptable especially when performing high resolution scans at low temperatures. Many tests were carried out but the source of the problem could not be located, with the result that the second system was selected as it did not suffer from this problem.

	InstaspecIV CCD & spectrograph	OMA4 CCD & American Holographic spectrograph
Spectral Range of the CCD	180-1100nm (UV enhanced)	400-1100nm
CCD Cooling	A single stage Peltier cooler. It can achieve -25°C using tap water as the coolant.	A three stage Petlier cooler. It can achieve -70°C using tap water as the coolant.
Dynamic Range (Analog to Digital Converter)	65,536:1 (16 bit)	262,144:1 (18 bit)
Software	The supplied software is very user friendly. A single program is all that is required to operate the CCD and perform any necessary analysis on the acquired spectrum.	The operation of this CCD is more complex as it requires two programs. The first program determines the order of events that are to occur when data is acquired and the second is used to call the first program and perform any necessary analysis on the recorded spectrum.
Calculation of the Wavelength Range being viewed.	This is carried out by the software and only requires the micrometer setting on the spectrograph and a known conversion factor (related to the grating).	This is also performed by the software but involves acquiring a spectrum of a suitable light source* and assigning the wavelength value of at least two of the spectral lines to the pixel values which they fall on.

** A suitable light source is one which has emission lines in the wavelength range of interest.*

Table 4.1 A list of some of the differences between the two CCD/spectrograph systems.

4.1 Suggested Improvements

The mapping system is at the early stages in its development and thus there are various improvements, described in this section, that can be performed to further increase its capabilities.

Some of the intensity maps, as stated in Chapter 3, were rendered useless by intermittent changes in the output power of the laser. This problem can be solved by using a facility available on the OMA CCD called source compensation. The basic principle behind this facility is that each time the CCD is triggered not only is a spectrum captured but the laser beam output power is sampled and the resultant value can be divided into the PL intensity, making this value independent of the laser output power and therefore unaffected by any fluctuations. This was not implemented as it involved further electronic and software development which could not be accomplished within the time scale of this project.

The time taken for a scan may be reduced by developing a handshaking technique between the xy stage and the CCD. Presently, the xy stage moves the laser beam a distance on the wafer and pauses for a predefined time while triggering the CCD to capture a spectrum. The length of the pause has to be long enough so that the CCD can record the spectrum and perform any necessary analysis before it receives the next trigger pulse from the xy stage. This is not the optimum way to operate because if the pause length is too short the CCD may not be ready when the next pulse arrives, causing it to be missed, or else there maybe use of overkill in the choice of the pause duration, resulting in a scan taking longer than it should. To improve this it would be better to get rid of the estimated pause time of the xy stage and replace it with the following:

- The xy stage moves the laser beam to a point on the wafer where it stops and triggers the CCD,
- The CCD captures a spectrum, performs the necessary analysis and then triggers the xy stage to move the laser beam to the next point on the wafer.

The DAS program that is currently used to set up the data acquisition mode of the OMA4 CCD was an example program as supplied by EG&G PARC and thus it is for general use with no specific project in mind. It could therefore contain functions

and tasks which may not necessarily be appropriate to this system and consequently would be a source of time delays. This slow scan time was not initially foreseen and thus the example program was used instead of writing a new DAS program more tailored to the system, as this would require an in-depth knowledge of the hardware functionality of both the computer and CCD electronics.

Reducing scan time will allow for further data analysis to be performed while the system is scanning. At the moment the need to measure values other than the peak intensity and the peak wavelength is outweighed by the time taken for a scan, which can be costly when working at cryogenic temperatures. Scans of step size smaller than 600μm will also become more feasible with a reduced scan time.

The next major step in the development of this system is to modify it so that along with PL a sample can be characterised using Raman scattering. This would allow for the characterisation of such parameters as the crystalinity, impurities and free carriers in a semiconductor, as discussed in [1]. The CCD is very suitable for the measurement of low light levels (Raman scattering) because of its low noise and high sensitivity, *i.e.* it is 100 times more sensitive than a photodiode array (PDA).

The measurable spectral range of the system could be extended to beyond 1μm by using array detectors such as InGaAs, PtSi or InSb. This would allow for the analysis of wafers using infrared spectroscopy, thereby facilitating the characterisation of silicon based wafers.

It would be worth investigating the possibility of running both the xy stage and the CCD from a single computer by incorporating the code for the xy stage into the program that runs the CCD.

Finally, there may be some benefit gained by having some form of wafer position indicator so that the xy stage could move the laser beam to any point on the wafer by simply entering in the x,y coordinates, as this would allow for more in-depth analysis of hot spot areas on a wafer.

4.2 Suggested Tests

As previously stated the objective of this project was to produce a system that facilitated the spatial and spectral characterisation of semiconductor wafers at various cryogenic temperatures using PL as the characterisation technique. Two separate

CCD/spectrograph configurations were tested and many factors such as reliability, available software functions, robustness and repeatability had to be examined in order to come to a decision on which one to select. Ultimately the deciding factor was, as stated in Section 4.0, the intermittent crashing of the InstaspecIV model. Due to time limits on the project this meant that other important tests could not be carried out. One key issue is the ultimate spatial resolution of the system which could be established using a resolution test target such as the USAF or the NBS test targets described in [2]. Secondly, a factor of particular significance for intensity maps is the spatial uniformity of the wafer mapping unit. A scan of the emission from a uniform light source at the wafer position would provide the necessary information and any observed non-uniformity could be used to normalize raw data.

4.3 Conclusion

In summary, the ability of the wafer mapping unit to characterise semiconductor wafers using PL has been successfully demonstrated at room, liquid nitrogen and liquid helium temperatures, as can be seen from the various peak wavelength and peak intensity maps, displayed in Chapter 3, of epilayer and quantum-well structures grown on GaAs wafers.

References

1. S. Perkowitz *Optical Characterization of Semiconductors: Infrared, Raman and Photoluminescence Spectroscopy*, Academic Press Limited, London, UK, 1993.
2. Melles Griot *Optics Guide 5*, 1990.

Appendix A

Note:

Any text between {} in the following three programs constitutes comments and does not appear in the actual programs.

The following program is used to control the motion of the xy translation table. The main part of the program is written in Quickbasic and is used to download the code used by the xy motor controller (NF90) to define the motion of the xy translation table.

5 CLS

10 OPEN "COM1:9600,E,7,2,CS,DS" FOR RANDOM AS #1

{This prepares the COM1 port on the computer for the transmission of data using a 9600 Baud rate. The COM1 port is connected to the NF90 via an RS-232 cable.}

20 PRINT #1, "FN"

{This puts the NF90 on-line.}

30 PRINT #1, "C S1M1000,S2M1000,I1M200,P10,L11,I2M200,S1M2000,I1M0,L10,R"

{This line downloads to the NF90 the code for the 60mm by 60mm raster scan.}

40 GOSUB 100

{This calls a subroutine that delays the program from going to line 50 until the 60mm by 60mm scan is completed.}

50 PRINT #1, "C I1M0,I2M0,R"

{This resets the motors of the xy translation table.}

60 GOSUB 100

70 PRINT "FINISHED"

```
80 PRINT #1, "Q"
{This puts the NF90 off-line.}

90 END

{The following three lines make up the delay subroutine. This routine will wait until
the computer receives the character ^ from the NF90, which it will transmit when the
motors have stopped.}
100 C$ = INPUT$(1, #1)
110 IF C$ <> "^" THEN 100
120 RETURN
```

The second program is an example of the type of program used by InstaspecIV system to set up the CCD and acquire data. The program records the peak intensity (maximum signal) and the corresponding peak wavelength for two separate pixel ranges, defined by the user (*i.e.* 0 to 280 and 282 to 450).

```
cls
c = 0

{The while loop ensures that 10,000 external trigger pulses are recorded before the
program ends.}
while(c < 10000)

    run(0,1,1,0,0.05,0,0,0,0)
    {This sets the CCD running in an external trigger mode with an exposure
    time of 50msec.}
    a = max(#sig,0,280)
    {This assigns the pixel number with the maximum signal (in the first pixel
    range) to variable a.}
```

```
        b = max(#sig,282,450)

        i = #sig[a]
        {This assigns the value of the signal at pixel a ( i.e. the peak intensity) to
        variable i.}

        w = xcal(#sig,a)
        {This calculates the corresponding wavelength of the pixel with the maximum
        signal and assigns it to variable w.}

        j = #sig[b]
        v = xcal(#sig,b)

        write("Waveln.dat",w,i,v,j)
        {This writes all the recorded data to the file Waveln.dat.}

        c = c + 1
        cls
wend
```

The final program is an example of the type of program used by the OMA4 system to set up the CCD and acquire data. It is written in a customised Pascal language. The program calculates the peak intensity and peak wavelength for two different pixel ranges, defined by the user.

```
program oma4;

var
s, p , c ,k ,l , d                  : integer;
dat_pt_num                          : integer;
out_file                            : text;
areac1, areac2                      : real;
count1, max1, max2                  : integer;
a1                                  : array[11000] of integer;
b1                                  : array[11000] of single;
a2                                  : array[11000] of integer;
b2                                  : array[11000] of single;
```

```
prompt_text                          : string;
low_lim, low_lim2, pix_range         : integer;


{This procedure is used to write text to the screen.}
procedure write_text;
begin
        buflen  := strlen(prompt_text);
        {This calculates the space required inorder to print the text stored in the
        variable prompt_text to screen.}
        writeln();
        write(prompt_text);
end;

{This procedure is used to find the peak intensity and peak wavelength in two
different pixel ranges.}
procedure line2;
begin

        buflen  := 20;

        {This while loop repeats until all external trigger pulses have been detected.}
        while(count1 < dat_pt_num) do
        begin
                d_run(0);
                {This sets the CCD running in an external trigger mode.}

                areac2  := D_AREA(0,0,255);
                {This finds the area under the curve between pixels 0 and 255 and
                assigns this value to the variable areac2.}

                {The following if statement is used to distinguish whether a new
                spectrum has been recorded by comparing the current spectrum with
                the spectrum in memory. This is necessary as the CCD unit would
                keep calculating the peak intensity and peak wavelength of the
                spectrum in memory even though the next external trigger has not
                been detected, i.e. the spectrum in memory has not been updated.}
                if (areac1 <> areac2 ) and (areac1 <> 0) then
                begin
                        replot_window();
                        {This plots the captured spectrum on the screen and in doing
                        so loads the spectrum into memory so that it can be analysed.}

                        max1    := 0;
                        max2    := 0;
```

```
                    {This for loop is used to scan through all the pixels, find the
                    pixel with the maximum signal in both ranges and assign the
                    pixel numbers to variables c and d respectively.}
                    for s    := 0 to pix_range do
                    begin
                            k       := low_lim + s;
                            l       := low_lim2 + s;

                            {CS[0].[0] refers to the spectrum captured and y[k]
                            refers to the y value in the spectrum at pixel number k
                            (k being an integer variable).}
                            if CS[0].[0].y[k] > max1 then
                            begin
                                    max1    := cs[0].[0].y[k];
                                    c       := k;
                            end;

                            if CS[0].[0].y[l] > max2 then
                            begin
                                    max2    := cs[0].[0].y[l];
                                    d       := l;
                            end;

                    end;

                    a1[count1]      := max1;
                    {This assigns the peak intensity, for range one, to the array
                    a1.}
                    b1[count1]      := cs[0].[0].x[c];
                    {This assigns the corresponding peak wavelength, for range
                    one, to the array b1}

                    a2[count1]      := max2;
                    b2[count1]      := cs[0].[0].x[d];
                    count1          := count1 + 1;
            end;
            areac1  := areac2;
    end;

    {The following four lines are used to write all the data from the scan to the
    file test2.dat.}
    assign(out_file,'test2.dat');
    for p := 0 to dat_pt_num-1 do
    writeln(out_file, a1[p], b1[p], a2[p], b2[p]);
    close(out_file);
end;
```

```
{ Main Program }
begin
        low_lim         := 0;
        low_lim2        := 0;
        pix_range       :=0;
        areac1          := 0;
        count1          := 0;
        a1              := 0;
        b1              := 0;
        a2              := 0;
        b2              := 0;
        c               := 0;
        d               := 0;
        k               := 0;
        l               := 0;

        prompt_text     := 'Enter in the number of data points -->';
        {For example, a 100 by 100 step scan would require 10,000 data points.}

        write_text();
        read(dat_pt_num);


        prompt_text     := 'Enter in the first lower limit -->';
        {The lower limit is the number of the first pixel in range one.}
        write_text();
        read(low_lim);

        prompt_text     := 'Enter in the second lower limit -->';
        write_text();
        read(low_lim2);

        prompt_text     := 'Enter in the pixel range -->';
        {The pixel range, or the number of pixels to be scanned, is the same for both
        ranges, resulting in only one for loop being required when calculating the
        peak intensity and peak wavelength.}

        write_text();
        read(pix_range);
        writeln();

        line2();
        {This is used to call procedure line2.}

        writeln('Finished');
end.
```

Appendix B

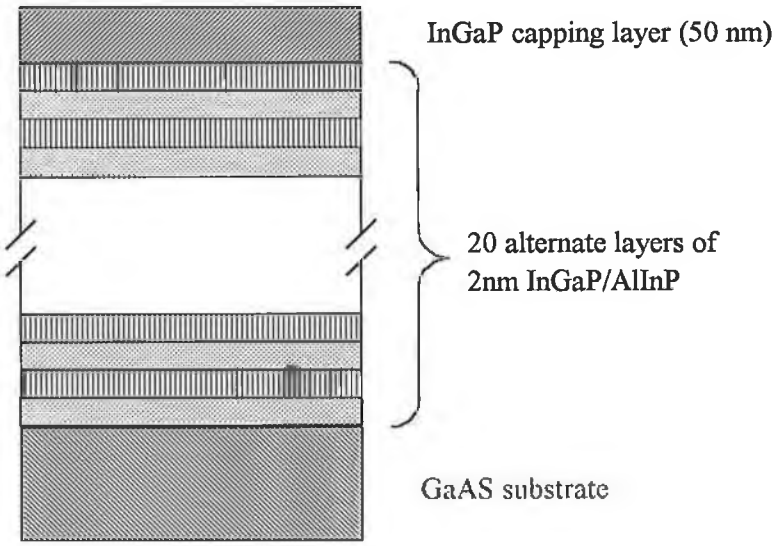

A schematic diagram of the structure of wafer B.

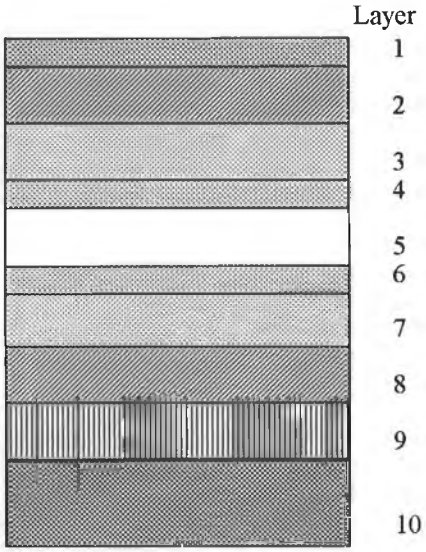

A schematic diagram of the structure of wafer C.

Layer	Description	Width
1	Low p-type Zn: GaAs capping layer	Not available
2	Undoped AlGaAs (43% Al)	870Å
3	Undoped AlGaAs (Al graded from 3% to 43%)	800Å
4	Undoped GaAs	Not available
5	InGaAs (18% In) Quantum Well	125Å
6	Undoped GaAs	Not available
7	Undoped AlGaAs (Al graded from 3% to 43%)	800Å
8	Si doped ($7x10^{17}$ cm^{-3}) AlGaAs (43% Al)	0.5μm
9	Si doped GaAs buffer layer	0.5μm
10	Si doped GaAs substrate	Not available